

1 **Exploring impacts of forest management strategies on water partitioning in a drought-sensitive catchment**
2 **using a tracer-aided ecohydrological framework**

3 Cong Jiang ¹, Doerthe Tetzlaff ^{1,2,3}, Songjun Wu ¹, Christian Birkel ^{1,4}, Hjalmar Laudon ⁵, Chris Soulsby ^{1,3,5,6}

4 ¹ Department of Ecohydrology and Biogeochemistry, Leibniz Institute of Freshwater Ecology and Inland Fisheries
5 (IGB), Berlin, Germany

6 ² Department of Geography, Humboldt University Berlin, Berlin, Germany

7 ³ Northern Rivers Institute, University of Aberdeen, Aberdeen, UK

8 ⁴ Department of Geography, University of Costa Rica, San Pedro, Costa Rica

9 ⁵ Department of Forest Ecology and Management, Swedish University of Agricultural Science (SLU), Umeå,
10 Sweden

11 ⁶ Chair of Water Resources Management and Modeling of Hydrosystems, Technical University Berlin, Berlin,
12 Germany

13 *Correspondence to:* Cong Jiang (cong.jiang@igb-berlin.de)

14 **Abstract.** Land use strongly influences water partitioning, water availability, and ecohydrological resilience in
15 drought-sensitive regions. Forest management plays a critical role through its effects on water use, which depends
16 on forest type, forest density, root water uptake, yet the ecohydrological consequences of different forest
17 management strategies—particularly in terms of blue and green water fluxes—remain poorly quantified. Here,
18 we develop and apply a parsimonious, tracer-aided forest management scenario framework using the conceptual
19 ecohydrological model EcoPlot-iso, designed to isolate the dominant vegetation-structural controls on long-term
20 water partitioning. We investigated how variations in generic forest type (e.g., broadleaf vs. conifer), forest density,
21 and root distribution influence water partitioning and ecohydrological resilience under different wetness
22 conditions in the drought-sensitive lowland Demnitzer Millcreek catchment (DMC), northeastern Germany.
23 Baseline simulations for the period 2000–2024 were conducted at three forest sites and used to develop forest-
24 type-specific reference conditions for comparison with alternative forest management scenarios. A key innovation
25 in this version of EcoPlot-iso was the integration of a depth-dependent root water uptake function, allowing
26 simulation of transpiration across soil layers under contrasting rooting distributions corresponding to different
27 stand ages. The model was calibrated and validated using seven years of soil moisture and three years of soil water
28 isotope ($\delta^2\text{H}$) data through a multi-criteria approach. Results showed that, on average, evapotranspiration was
29 highest under conifers, exceeding broadleaf forests and agroforestry by 7% and 11%, respectively, while
30 agroforestry exhibited the greatest groundwater recharge. Significant differences in water partitioning between
31 dry and wet years were observed across management scenarios. Conifer forests showed stronger transpiration
32 contrasts than broadleaf forests in early spring, while the wet–dry-year contrast between the two forest types was
33 largest in late spring. Our findings highlight the potential of agroforestry, such as crop–tree mixtures, to mitigate
34 drought impacts on soil water availability and groundwater recharge. Overall, this study demonstrates how a
35 parsimonious, tracer-aided scenario framework can be used as a decision-support tool to quantify and visualize
36 the effects of land use change on water availability in data-limited regions, supporting more informed decision-
37 making and enhanced ecohydrological resilience under increasing drought pressure.

38

39 **1 Introduction**

40 Land use plays a crucial role in regulating water, carbon, energy, and nutrient cycles by mediating ecohydrological
41 fluxes and soil water storage dynamics which link interactions between the atmosphere, soils, vegetation and
42 biogeochemical processes (Mahmood et al., 2014; Pielke et al., 2011; Smith et al., 2021; Sterling et al., 2013).
43 Among the different types of land cover, forests are particularly important elements of the land use mosaic,
44 providing a range of ecosystem services, including enhancing infiltration, stabilizing soils, storing carbon,
45 supplying timber and fuelwood, as well as buffering extreme climate events (Bonan, 2008). However, there are
46 clear trade-offs, as forests and trees also tend to use more water than contrasting land uses (Bosch and Hewlett,
47 1982; Calder, 1998). This is because their high Leaf Area Index (LAI) and canopy storage capacities often result
48 in greater interception losses and canopy evaporation, while their deeper and denser rooting networks can sustain
49 transpiration when top soils dry out (Wang-Erlandsson et al., 2014). Consequently, forest management decisions
50 (e.g., afforestation, thinning, and forest type selection) can significantly affect water yield and the partitioning
51 into blue water fluxes (runoff and groundwater recharge) and green water fluxes (evapotranspiration), as well as
52 the ecohydrological resilience to drought. Here, ecohydrological resilience is defined as the ability of the soil–
53 plant–water system to maintain key ecohydrological functions, including soil moisture storage, transpiration, and
54 groundwater recharge, under drought stress (Falkenmark and Rockström, 2006; Neill et al., 2021; Tetzlaff et al.,
55 2024).

56 Sustainable land management also requires consideration of sensitivity to climate change, which is altering
57 hydroclimatic regimes by shifting precipitation patterns and increasing atmospheric moisture demand (Huntington,
58 2006; Trenberth, 2011). These changes can intensify drought frequency and duration, increase evaporative losses,
59 and reduce groundwater recharge and surface water availability, thereby exacerbating water scarcity in many
60 regions (Ault, 2020; Yuan et al., 2023). Because land use practices—particularly forest management—are
61 expected to strongly influence water partitioning, it is important to assess their impacts under changing
62 hydroclimatic conditions in order to evaluate the ecohydrological resilience of soil–plant–water systems,
63 especially in drought-sensitive areas.

64 The understanding of how land use change affects runoff generation, soil moisture storage and evapotranspiration
65 dynamics has gradually developed through decades of research, including long-term paired experimental
66 watershed investigations of water yield (Bosch and Hewlett, 1982; Brown et al., 2005, 2013; Hibbert, 1967).
67 However, quantifying the impact of forest management on water partitioning remains challenging in most
68 situations (Guswa et al., 2020). This is due to the complex interplay of climate conditions, soil properties,
69 vegetation type, and topography, and the difficulty in distinguishing individual evapotranspiration (ET)
70 components (Kool et al., 2014; Smith et al., 2021; Zhang et al., 2001). These challenges are further compounded
71 by scarce long-term observational data for forest ecosystems, which are essential given their slow dynamics and
72 lengthy growth cycles (Tetzlaff et al., 2017).

73 In forest ecosystems, ET is particularly challenging to simulate due to complex interactions among canopy
74 structure, stomatal behavior, and root water uptake (Tague and Band, 2004). Many ecohydrological models
75 include some form of root water uptake parameterization (e.g., mHM, Ech2O-iso, RHESSys), in which canopy
76 transpiration is typically constrained by surface energy balance and stomatal conductance and subsequently
77 distributed among soil layers based on soil water availability and root distribution. While such models provide

78 detailed representations of land–atmosphere and soil–vegetation interactions, their application in forest
79 management studies is often constrained by high data requirements, computational demand, and parameter
80 uncertainty, particularly in data-scarce regions (Fatichi et al., 2012; Ricci et al., 2020; Tague and Band, 2004). In
81 this context, conceptual tracer-aided ecohydrological models can provide a complementary, process-based, and
82 practical framework for systematically exploring long-term forest management impacts on water partitioning and
83 ecohydrological resilience (Landgraf et al., 2023). By integrating climatic forcing, canopy structure (e.g., leaf area
84 index), soil moisture dynamics, and stable water isotopes, such approaches facilitate robust assessment of green-
85 and blue-water fluxes under contrasting forest management scenarios (Neill et al., 2021).

86 In this study, we apply the tracer-aided conceptual model EcoPlot-iso to assess how land use, specifically forest
87 management strategies, influences water partitioning and soil moisture storage in the drought-sensitive, lowland
88 Demnitzer Millcreek catchment, NE Germany. This lowland catchment is typical of large areas in central Europe
89 where freely draining, sandy soils combine with relatively low precipitation, and high evaporative demand amplify
90 drought stress under climate change. To improve the quantification of transpiration, we introduce a novel
91 development in EcoPlot-iso by integrating a depth-dependent root water withdrawal function into the transpiration
92 equation. The model is dual-calibrated and validated using seven years of soil moisture data and three years of
93 soil water isotope data. A series of generic forest management scenarios — varying broad forest types (broadleaf,
94 coniferous, agroforestry), forest density, and rooting characteristics — are developed within a parsimonious,
95 tracer-aided forest management scenario framework, to explore their impacts on vertical water fluxes and
96 ecohydrological resilience.

97 This study aims to answer the following research questions:

- 98 ➤ How does vegetation cover influence water use and partitioning under varying wetness conditions
99 in a drought-sensitive, lowland catchment?
- 100 ➤ What are the implications of alternative generic forest management scenarios for water availability
101 and overall ecohydrological resilience?
- 102 ➤ How can land management strategies be optimized to reduce drought impacts on soil water
103 availability and groundwater recharge and enhance ecohydrological resilience under climate change?

104 **2 Study area**

105 **2.1 Demnitzer Millcreek catchment (DMC)**

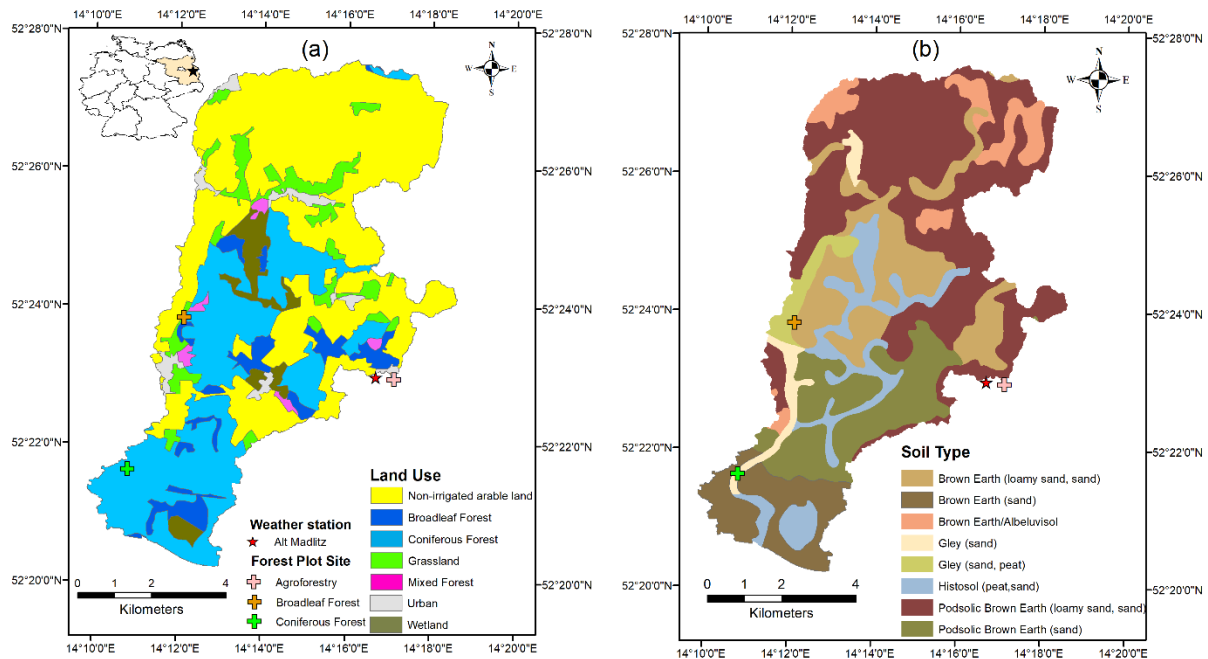
106 The Demnitzer Millcreek catchment (DMC) is a 66 km² lowland basin (30–90 m elevation) in the State of
107 Brandenburg, Germany, approximately 55 km east of Berlin (52°23' N, 14°15' E) (Fig. 1). Located in the Northern
108 European Plain, it is part of a drought-sensitive region that provides many essential ecosystem services, including
109 agriculture, timber production, and water supply.

110 The DMC landscape is dominated by non-irrigated farmland, mostly arable crops and some grazing on more
111 water-retentive brown earth and gley soils respectively which cover 60% of the catchment (Fig. 1a and b). Forests
112 cover 36% of the catchment on more freely draining sandy soils, and include coniferous, broadleaf, and mixed
113 stands. Small urban settlements (2%) are scattered throughout the catchment, with wetlands on peat soils primarily

114 found along streams in the central part of the catchment. The climate is temperate with warm summers, with a
115 mean annual temperature of 9.6°C and average precipitation of approximately 558 mm, based on weather station
116 data from 2000 to 2024. Potential evapotranspiration (PET) ranges from 584 to 789 mm per year from 2000 to
117 2024, based on calculations from this study (see Section 3.3). Interannual variability in precipitation, including
118 the identification of dry and wet years, is shown in Fig. S1, which highlights deviations from the long-term mean
119 and helps contextualize recent drought impacts. Rainfall peaks in summer, accompanied by intense convective
120 storms; however, surface runoff is rare, as the soils are highly permeable and dry in the growing season.
121 Consequently, the catchment is primarily groundwater-dominated with winter high flows and often dries in the
122 summer (Smith et al., 2021). The geology consists mainly of glacial and fluvial deposits and base moraines, while
123 the dominant soil types include poorly drained silty gley brown earth and well-drained podzolic brown earth soils
124 (Fig. 1b).

125 The DMC has a long history of human influence, with significant land use changes affecting its hydrology. In the
126 18th Century, artificial drainage channels were constructed to convert wetlands into agricultural land. Since the
127 1990s, efforts in wetland restoration and wildlife recolonization (e.g., beaver recovery) have aimed to enhance
128 water retention in the landscape. Long-term hydrological and isotopic monitoring (Gelbrecht et al., 1996, 2005;
129 Smith et al., 2020; Wu et al., 2021) has provided valuable insights into the impacts of agriculture and land use
130 management on water quality, ecohydrological partitioning and soil water storage. The 2018 European drought
131 and subsequent prolonged dry periods have exacerbated water scarcity and ecosystem vulnerability (Kleine et al.,
132 2021). In response, some land owners have explored agroforestry and other adaptive forest and tree management
133 strategies to improve water retention and reduce drought vulnerability (Luo et al., 2024). Agroforestry represents
134 a transitional system blending low density tree cultivation with agriculture; either in terms of grazing the
135 understory vegetation or crops (Landgraf et al., 2022; Quandt et al., 2023). Given the long-term monitoring record
136 and ongoing land use change, DMC serves as a useful site for assessing the impacts of changing forest
137 management on water partitioning, soil moisture and ecohydrological resilience under different wetness
138 conditions.

139



140
 141 **Figure 1.** Location, land use (a) and soil type (b) map of the Demnitzer Millcreek catchment, showing the current
 142 distribution of broadleaf forests, conifer forests, agroforestry, cropland, and grassland.

143 **2.2 Forest Plot Sites**

144 To investigate the effects of forest management scenarios on water partitioning and ecohydrological resilience,
 145 three predominantly forest plot sites — broadleaf forest, conifer forest and agroforestry — were selected within
 146 the drought-sensitive DMC. These plots represent contrasting forest types central to the modelling experiments.
 147 The plot locations are shown in Fig. 1, and key site characteristics are summarized below, with further details
 148 available in Kleine et al. (2021) and Landgraf et al. (2023). A summary of observed soil types and soil moisture
 149 monitoring characteristics for these three forest sites is provided in Table 1, which also highlights pronounced
 150 differences in long-term mean volumetric soil moisture averaged over the 0–1 m soil profile, with values highest
 151 in agroforestry (~21%), intermediate in broadleaf (~11%), and lowest in conifer forest (~5.5%).

152 The broadleaf forest site represents a relatively mature forest system (~60 years old) and is dominated by mature
 153 European oak (*Quercus robur*) with a few Scots pine (*Pinus sylvestris*) present within the plot. Additional species
 154 including Norway maple (*Acer platanoides*), elm (*Ulmus* spp.), and hazel (*Corylus avellana*) are found within
 155 10 m of the plot boundary. The soil is classified as brown earth, with a loamy sand to sand texture.

156 The conifer forest site is structurally simpler and more homogeneous, and is dominated by mature Scots pine
 157 (*Pinus sylvestris*) plantation. A limited number of broadleaf species, such as European oak and Norway maple,
 158 are also present within the plot, reflecting a conifer-dominated canopy. The soil is a weakly developed brown
 159 earth, characterized by coarse sandy texture and overlying gravels.

160 The agroforestry site represents a transitional system between forest and agriculture and is characterized by
 161 minimal canopy cover and no irrigation. It consists of rows of small deciduous trees or shrubs (≤ 2 m in height),

162 spaced approximately 2–3 m apart, interplanted with rainfed legumes (Landgraf et al., 2023). The soil is classified
 163 as podsollic brown earth, with a loamy sand to sand texture.

164 Together, these three sites represent a realistic gradient of forest land use intensity and provide a basis for
 165 exploring how forest type, forest density, and rooting depth affect ecohydrological responses under varying
 166 climatic conditions.

167 **Table 1.** Summary of observed soil types and soil moisture data at the three forest sites.

Site	Soil Type	Texture	Layer	Soil Moisture (mm)				Period
				Max	Min	Mean	SD	
Broadleaf forest	Brown earth	Loamy sand/sand	0 to 10 cm	26.3	3.5	13.7	6.3	2018.6-2024.12
			10 to 30 cm	56.2	6.9	24.7	11.7	
			30 to 100 cm	147.5	25.8	71.7	33.5	
Conifer forest	Sandy brown earth	Coarse sand	0 to 10 cm	28.7	8.6	17.3	7.1	2019.3-2024.12
			10 to 30 cm	53.8	2.6	21.8	12.3	
			30 to 100 cm	34.7	2.7	15.9	8.0	
Agroforestry	Podsollic brown earth	Loamy sand/sand	0 to 10 cm	32.1	10.4	21.3	7.8	2019.3-2024.12
			10 to 30 cm	53.4	7.2	29.8	13.5	
			30 to 100 cm	223.6	86.8	163.4	42.0	

168 3 Method and Data

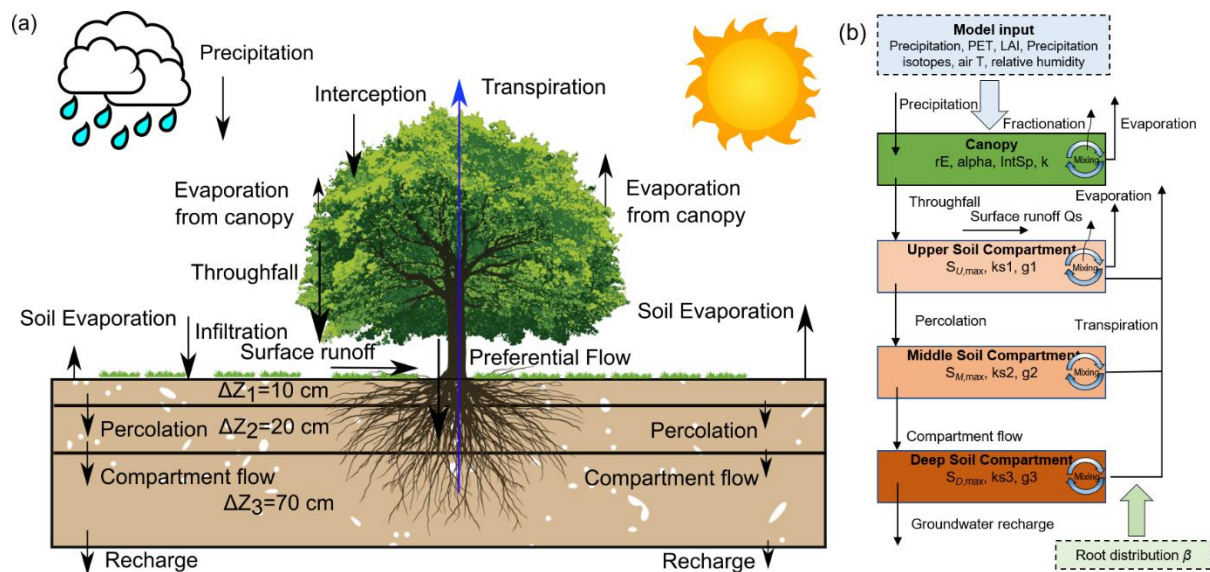
169 3.1 Model Framework and Structure

170 This study employs the EcoPlot-iso model, a tracer-aided ecohydrological modelling framework designed to
 171 simulate key ecohydrological and isotopic processes that characterise water partitioning at the plot scale (Birkel
 172 et al., 2024; Landgraf et al., 2023; Stevenson et al., 2023). EcoPlot-iso is a process-based conceptual model that
 173 simulates key ecohydrological fluxes, including interception, throughfall, infiltration, preferential flow, surface
 174 runoff, percolation, and groundwater recharge, as well as evapotranspiration components such as canopy
 175 evaporation, soil evaporation, and transpiration (Fig. 2a). These processes are represented within a vertical
 176 structure comprising a single canopy layer and three soil layers (0–10 cm, 10–30 cm, and 30–100 cm) (Fig. 2b).
 177 The vertical discretization follows the established EcoPlot-iso configuration and effectively represents vertical
 178 gradients in soil moisture and isotopic composition, broadly consistent with soil moisture and isotope
 179 measurements within each layer. Recently, the isotope tracking module was further developed to include
 180 fractionation and mixing processes, allowing EcoPlot-iso to better constrain the partitioning between evaporation
 181 and transpiration and improve water flux estimates. The required input variables (Table 2) include meteorological
 182 data such as precipitation, potential evapotranspiration (PET), air temperature, and relative humidity, along with
 183 stable water isotopic data (precipitation isotope) and vegetation-related parameters (leaf area index, LAI).

184 In EcoPlot-iso, canopy surface cover fraction (SCF) is derived from LAI using Beer’s law with an extinction
 185 coefficient rE (Eq. S1). Maximum canopy storage is determined by the SCF and an interception threshold
 186 parameter α . Interception is represented by a nonlinear saturation-type function (Eq. S2), whereby precipitation is
 187 first stored in the canopy until maximum canopy storage is reached, and any excess is routed as throughfall.
 188 Potential evapotranspiration PET is partitioned into canopy and soil fractions according to SCF (Eqs. S3 and S4).
 189 The canopy fraction drives evaporation from the interception store and transpiration from the soil layers, while
 190 the soil fraction drives evaporation from the upper soil layer (Eqs. S5–S6). Actual fluxes are constrained by water

191 availability: interception evaporation depends on canopy storage, transpiration is sequentially satisfied from the
 192 upper to deeper soil layers according to the relative soil-moisture availability (STO/S_{max}) of each layer (Eqs. S7–
 193 S9), and soil evaporation is limited by moisture availability in the upper soil. Surface runoff is represented using
 194 a Hortonian threshold approach, where precipitation in excess of infiltration capacity is routed as runoff (Eq. S10).
 195 Preferential flow is triggered when throughfall exceeds a threshold, with a calibrated parameter controlling the
 196 bypass proportion (Eq. S11). Percolation, compartment flow and groundwater recharge are represented as storage–
 197 discharge relationships, where outflows are parameterised as power functions of soil or groundwater storage (Eqs.
 198 S12-S14). Groundwater recharge is defined as the downward percolation flux at the lower boundary of the soil
 199 domain (30–100 cm layer), corresponding to a total soil depth of 1 m. Full variable definitions and governing
 200 equations are provided in Table S1 of the Supplementary Material (Eqs. S1–S14).

201 EcoPlot-iso has been applied in diverse climatic and hydrological settings, including a one-year simulation in
 202 Scotland (Stevenson et al., 2023), a one-year simulation at the Demnitzer Millcreek (DMC) site in the Northern
 203 European Plain (Landgraf et al., 2023), and a four-year simulation in the humid tropics of Costa Rica (Birkel et
 204 al., 2024). Building on these applications, this study employs EcoPlot-iso for a long-term tracer-aided
 205 ecohydrological simulation to assess the effects of different forest management scenarios on water partitioning
 206 and ecohydrological resilience.



207
 208 **Figure 2.** (a) Schematic representation of the ecohydrological fluxes and water partitioning in the EcoPlot-iso
 209 model illustrating major water fluxes and storage components; (b) Conceptual framework and key parameters of
 210 the EcoPlot-iso model (Landgraf et al., 2023; Stevenson et al., 2023), highlighting the key ecohydrological
 211 processes simulated in this study.

212 3.2 Model Adaptations: Integrating Root Distribution into the Transpiration Equation

213 Although root water uptake plays a critical role in soil–plant–atmosphere interactions, the vertical rooting
 214 distribution and the associated depth-dependent uptake efficiency were not explicitly represented in EcoPlot-iso
 215 (Stevenson et al., 2023). The current study introduces a novel depth-dependent root uptake function to improve
 216 the model’s simulation of transpiration and water partitioning across different root distributions. This adaptation
 217 enables the model to account for variations in rooting depth and water uptake efficiency across land use types—
 218 such as young and mature forests or contrasting vegetation covers—that affect soil water extraction. Specifically,

219 a new transpiration equation was implemented to calculate root water uptake across three soil compartments—
 220 upper, middle, and deep—by incorporating depth-specific uptake efficiency:

$$221 \quad T_{p1} = r_{L1} * (T_P - E_i) * \left(\frac{S_U}{S_{U,\max}} \right) \quad (1)$$

$$222 \quad T_{p2} = r_{L2} * (T_P - E_i - T_{p1}) * \left(\frac{S_M}{S_{M,\max}} \right) \quad (2)$$

$$223 \quad T_{p3} = r_{L3} * (T_P - E_i - T_{p1} - T_{p2}) * \left(\frac{S_D}{S_{D,\max}} \right) \quad (3)$$

224 where T_{p1} , T_{p2} , T_{p3} represent the transpiration from the upper, middle, and deep soil compartments, respectively.
 225 T_p denotes the canopy fraction of potential evapotranspiration. E_i denotes the canopy evaporation. S_U , S_M , S_D
 226 represent the water storage in the upper, middle, and deep soil compartments. $S_{U,\max}$, $S_{M,\max}$, $S_{D,\max}$ are the
 227 maximum water storage capacities of these compartments. r_{L1} , r_{L2} and r_{L3} represent the root water withdrawal
 228 efficiency in the upper, middle, and deep soil compartments, respectively.

229 To explicitly link root water uptake to soil moisture availability and transpiration demand, an efficiency factor $r(z)$
 230 was introduced. The exponential root water withdrawal efficiency function is defined as:

$$231 \quad r(z) = e^{-\beta z} \quad (4)$$

232 where $r(z)$ represents the capacity of roots to extract water at depth z , and β is the decay rate (m^{-1}), which
 233 determines how quickly root activity decreases with increasing depth. A higher β value concentrates root activity
 234 near the surface, while lower β values allow for deeper water uptake (see Fig. S2 in Supplement). This formulation
 235 builds on the common assumption that potential root water uptake decreases exponentially with depth (Li et al.,
 236 1999; Wu et al., 1999) and is intentionally simplified for a plot-scale, data-constrained model setup. The soil
 237 profile is discretized into three layers (0–10 cm, 10–30 cm, and 30–100 cm; Fig. 2a), and r_{L1} , r_{L2} , and r_{L3} are
 238 calculated by evaluating $r(z)$ at the midpoint depth of each layer ($z = 5, 20, \text{ and } 65$ cm, respectively). These layer-
 239 specific efficiency values are then used as weighting coefficients in Eqs. (1)–(3) to calculate transpiration from
 240 each of the three soil compartments.

241 3.3 Model Setup, Input and Observation Data

242 The EcoPlot-iso model was applied to DMC across five sites with different dominant land use: broadleaf forest,
 243 conifer forest, agroforestry, cropland and grassland over a 25-year period (2000–2024) at daily timesteps. Soil
 244 moisture initialization was based on observed data, and a one-year spin-up period was included before each
 245 simulation to stabilize initial conditions. The input datasets required for the model—climate, vegetation, soil
 246 moisture, and stable water isotope data—are summarized in Table 2. Climate variables, including precipitation,
 247 temperature, wind speed, and relative humidity, were primarily obtained from the Müncheberg weather station
 248 (DWD, German Weather Service, ~20 km from DMC). Potential Evapotranspiration (PET) was calculated using
 249 the FAO Penman-Monteith equation, while net radiation was derived from ERA5 reanalysis data (Hersbach et al.,

250 2020). The Leaf Area Index (LAI) time series was extracted from the MODIS 8-day LAI product at the location
 251 of each study site and linearly interpolated to daily timesteps. To improve accuracy and reduce data noise, the
 252 MODIS LAI was further bias-corrected against in-situ LAI measurements (maximum and minimum values),
 253 following Smith et al. (2021) and Wu et al. (2023). Given the plot-scale setup of EcoPlot-iso, agroforestry systems,
 254 characterized by mixed crop–tree vegetation, are represented implicitly using MODIS-derived LAI and calibration
 255 against plot-scale soil moisture and isotope observations, rather than explicitly resolving multiple vegetation types.
 256 In addition, the complete set of time series input data used to drive the EcoPlot-iso simulations in the Demnitzer
 257 MillCreek Catchment for 2000–2024—including daily precipitation, precipitation isotopes ($\delta^2\text{H}$), air temperature,
 258 relative humidity, Leaf Area Index (LAI), and potential evapotranspiration (PET)—is presented in Figure S3 of
 259 the Supplementary Material.

260 Surface soil moisture (0–10 cm) was measured using a handheld soil moisture device (Theta handheld probe ML3
 261 Sensor) on a monthly basis during two field observation periods (2018–2019 and 2021). For subsurface soil
 262 moisture, permanently installed probes were used: SMT-100 at forest and grassland sites, and CS650 at
 263 agroforestry and cropland sites. Measurements were recorded at 15-minute intervals with two replicates per depth.
 264 To facilitate data processing and consistency, all soil moisture datasets were aggregated into daily mean values,
 265 resulting in one volumetric water content value per site and soil depth. Details of the measurement devices, depth
 266 intervals, and aggregation methods are summarized in Table S2. Daily precipitation samples for stable water
 267 isotope analysis from June 2018 onward were collected at the Hasenfelde AWS, and earlier data were obtained
 268 from the Berlin weather station. Soil water isotopes were sampled from bulk soil at the four plot sites at five
 269 depths (0–5, 5–10, 10–20, 20–30, and 30–50 cm) every 3–4 weeks during the growing season. The isotope data
 270 were aggregated according to the thickness of the corresponding model soil compartments. All isotope values are
 271 reported relative to Vienna Standard Mean Ocean Water (VSMOW). Further details on site instrumentation and
 272 data collection are described in Landgraf et al. (2022).

273 **Table 2.** Summary of the used climate, vegetation, soil moisture, and isotope data.

Data	Unit	Period	Timestep	Acquisition
<i>Climate data</i>				
Precipitation	mm/d	2000-2024	Daily	Muencheberg weather station (52.52°, 14.12 °)
Temperature	°C			
Windspeed	m/s			
Relative humidity	%			
Net shortwave radiation	W/m ²		Hourly	ERA5
Net longwave radiation				
Potential evapotranspiration	mm/d	Daily	FAO Penman-Monteith equation	
<i>Vegetation data</i>				
Leaf area index	-	2000-2024	8-days	MODIS at broadleaf forest, coniferous, and agroforestry sites
<i>Soil data</i>				
Soil moisture	%	2018-2024	Daily	broadleaf forest, cropland, agroforestry, and grassland sites
<i>Isotope data</i>				
Precipitation isotope $\delta^2\text{H}$	‰	2000-2024	Daily	Hasenfelde (52.41°N, 14.19°E), weather station in Berlin

Soil water isotope		2018-2019, 2021	Daily	Manually at broadleaf forest, cropland, agroforestry, and grassland sites
--------------------	--	--------------------	-------	---

274

275 3.4 Model Calibration and Validation

276 The EcoPlot-iso model was calibrated using the Monte Carlo approach combined with a multi-criteria evaluation
 277 based on soil moisture and soil water isotope observations at each land use site. For each calibration, 100,000
 278 parameter sets were generated using the Latin Hypercube Sampling (LHS) within a Monte Carlo framework
 279 (McKay et al., 1979) to broadly sample the parameter space and capture a wide range of plausible model behaviors.

280 The initial parameter ranges were defined based on literature values and site-specific knowledge. Specifically,
 281 initial ranges for the radiation extinction factor (rE) were guided by vegetation-specific light attenuation
 282 coefficients from canopy gap-fraction theory (Larcher, 1975; Gigante et al., 2009), using typical reference values
 283 of 0.35 for grasslands, 0.45 for croplands, and 0.65 for forests. Initial ranges for the interception storage capacity
 284 parameter (α) were guided by scaling values reported in global syntheses of canopy interception storage (Zhong
 285 et al., 2022) and interception sensitivity studies (Barnard et al., 2014), accounting for differences in model time
 286 step and formulation. The resulting interception evaporation is consistent with observational studies indicating
 287 that canopy interception losses typically represent approximately 10–30% of annual precipitation in forested
 288 systems (Staelens et al., 2008; Llorens & Domingo, 2007).

289 Model performance was evaluated using the modified Kling-Gupta Efficiency ($mKGE$) (Kling et al., 2012),
 290 calculated separately for soil moisture ($mKGE_{sm}$) and soil water isotopes ($mKGE_{iso}$) at each of the three soil depth
 291 layers. Calibration followed a two-step refinement process. In the first step, based on the initial parameter ranges,
 292 parameter sets were retained only if they fell within the intersection of the top 60th percentile of all six individual
 293 $mKGE$ metrics (i.e. soil moisture and soil water isotopes at each of the three soil depths). This step substantially
 294 reduced the number of parameter sets from the initial 100,000 samples. This intersection-based filtering ensured
 295 that retained simulations performed consistently well across all evaluated variables and depths. By retaining only
 296 the performance metrics and corresponding parameter sets, this step efficiently screened the parameter sets while
 297 substantially reducing data storage requirements during the initial exploration.

298 In the second step, the model was re-run using the retained parameter sets obtained from Step 1. For these re-run
 299 simulations, an average $mKGE$ value across depths and variables was then used as the objective performance
 300 metric (Eq. 5), and the 100 best-performing simulations were selected for final analysis. The model parameters,
 301 their initial ranges, and the refined ranges for each of land use are summarized in Table S3 in the Supplement. To
 302 assess parameter constraints and equifinality, the probability density distributions and median values of the
 303 calibrated parameters were derived from the 100 best-performing simulations for each site (see Fig. S4). These
 304 were then used to evaluate the convergence of the parameters relative to their initial ranges.

$$305 \quad mKGE = \frac{\sum_i^3 mKGE_{sm} + \sum_i^3 mKGE_{iso}}{6} \quad (5)$$

306 Model parameters were calibrated using the full available observation, comprising seven years of soil moisture
 307 data and three years of soil water isotope data, in order to maximise information content under limited isotope

308 availability (Shen et al., 2022). To additionally assess model robustness beyond a shorter calibration window, a
309 split-sample calibration–validation experiment was conducted consistently across all land-use types. In this
310 experiment, the model was calibrated using an earlier subset of the soil moisture and isotope observations,
311 followed by validation against an independent soil moisture period, as isotope observations were not available for
312 validation. Results from this split-sample evaluation, which showed good parameter transferability across most
313 sites, are reported in Table S4 and Figures S5–S7 of the Supplement. Given this transferability, the full-period
314 calibration was retained for the main scenario simulations, as it provides more stable parameter estimates under
315 data limitations, while the split-sample results are presented for transparency and robustness assessment.

316 **3.5 Development and Application of a Generic Forest Management Scenario Framework**

317 The primary goal of this study was to develop a new, parsimonious and generic forest management scenario
318 framework to evaluate how forest type, forest density, and root distribution —associated with forest age—
319 influence long-term water partitioning and ecohydrological resilience under comparable environmental conditions.
320 This framework was designed to capture the dominant effects of vegetation structure—such as interception and
321 transpiration through canopy and root networks—on water partitioning, rather than to reproduce detailed species-
322 specific physiology.

323 Based on this conceptual framework, baseline simulations covering the period 2000-2024 were established using
324 EcoPlot-iso model at three forest sites within the DMC (broadleaf forest, conifer forest, and agroforestry). These
325 baseline simulations provide forest-type–specific reference conditions against which alternative management
326 scenarios were evaluated.

327 To isolate the effects of forest management from site-specific soil properties and boundary conditions, we
328 extended the observed forest-site configurations by systematically combining forest-type–specific vegetation
329 parameter sets with site-specific soil parameter sets, derived from the corresponding baseline calibrations,
330 resulting in a 3×3 scenario matrix (Fig. 3). The diagonal entries represent the observed site-based reference
331 configurations—namely, Broadleaf forest site, Conifer forest site, and Agroforestry site —and are therefore
332 treated as baseline scenarios. The remaining cross-combinations represent hypothetical but plausible forest-site
333 (soil) configurations, in which vegetation characteristics are applied to alternative site-specific soil hydraulic
334 properties and boundary conditions (e.g., soil texture and compaction). This design enables vegetation effects to
335 be assessed independently of site-specific controls for scenario analysis, while acknowledging that vegetation and
336 soil controls may not be fully independent and that soil hydraulic properties and boundary conditions remain
337 inherently site-dependent. Ensemble-based comparisons across site configurations for each forest type therefore
338 support a more robust and generic interpretation of ecohydrological behaviour.

339 Specifically, for each of forest-site baseline scenario calibration, we retained the top 100 best-performing
340 simulations—ranked by average mKGE—and their corresponding parameter sets (as described in Section 3.4).
341 Forest-type–specific vegetation parameters (rE , α) were derived from site-specific calibrations for broadleaf,
342 conifer, and agroforestry systems, and their median values from the 100 best-performing simulations at each site
343 were used to represent characteristic vegetation conditions. The root distribution parameter (β) was not treated as
344 strictly vegetation-specific, but as jointly influenced by vegetation type, soil properties, and soil water availability
345 (Fig. S4). This ensemble-based selection was used to reduce parameter uncertainty and equifinality effects. These

346 calibrated parameter sets were then used for subsequent scenario simulations to ensure physically consistent
347 parameter configurations across all forest types. In contrast, soil-related parameters (ks_1 , ks_2 , ks_3 , $S_{U,max}$, $S_{M,max}$,
348 $S_{D,max}$, I_c , g_1 , g_2 , g_3 , $PFscale$) were retained from the corresponding forest sites to preserve site-specific hydraulic
349 properties and boundary conditions.

350 For vegetation forcing, we used forest-type-specific observed LAI time series (broadleaf, coniferous, and
351 agroforestry), derived from the MODIS LAI products, described in Section 3.3 (Table 2; Fig. S3d). Forest-type-
352 specific initial soil moisture conditions for the three soil layers were kept consistent with the corresponding
353 baseline simulations. All scenario simulations were driven using identical climate input data, precipitation isotope
354 time series, and potential evapotranspiration forcing as the baseline simulations to isolate the effects of forest
355 characteristics and management.

356 The scenario framework varied three key dimensions of forest management:

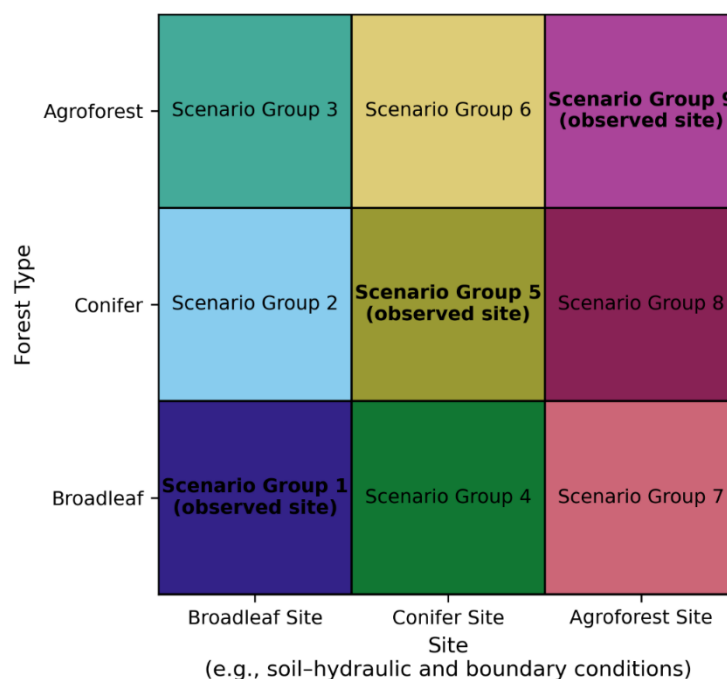
- 357 a) Forest type was varied by implementing three canopy types—broadleaf, conifer, and agroforestry—each
358 assigned type-specific vegetation parameters and LAI time series to reflect differences in canopy
359 structure.
- 360 b) Forest density was varied by multiplying the reference LAI by a scaling factor ranging from 0.2 to 1.8.
361 Higher forest density was represented by scaling factors >1.0 , indicating denser canopy cover, while
362 lower forest density corresponded to factors <1.0 , reflecting more open canopy conditions. The applied
363 LAI scaling range (0.2–1.8) follows previous tracer-aided modelling approaches (Neill et al., 2021) and
364 spans realistic management-induced variability in canopy density, while remaining consistent with
365 reported LAI values for mature European forests (Leuschner et al., 2006).
- 366 c) Root water uptake efficiency was varied by scaling the site-calibrated β parameter to represent
367 contrasting vertical root distributions associated with forest developmental stage. Three rooting scenarios
368 were considered: $0.5 \times \beta$, $1.0 \times \beta$, and $2.0 \times \beta$, where β is the calibrated value for each forest site. Lower
369 scaled values ($0.5 \times \beta$) represent more developed forests with deeper, less surface-weighted rooting
370 systems, while higher scaled values ($2.0 \times \beta$) represent younger or less-developed forests with shallower,
371 more surface-weighted rooting distributions (see Fig. S1). The $1.0 \times \beta$ scenario corresponds to the
372 observed rooting distribution at each forest site.

373 Within this framework, LAI and rooting distribution were treated as independent scenario dimensions. LAI scaling
374 represented management-induced changes in canopy density, whereas rooting distribution scenarios reflected
375 contrasts in belowground water uptake. Their combined effects on water fluxes were evaluated without assuming
376 a fixed linkage between canopy structure and rooting depth. This separation acknowledges that canopy density
377 can change rapidly through management (e.g., thinning or harvesting), while rooting characteristics typically
378 reflect longer-term stand development, thereby allowing realistic representation of above- and belowground
379 controls on water partitioning.

380 Although EcoPlot-iso was originally developed for plot-scale applications, it is applied here to represent
381 ecohydrological fluxes in a range of well-characterized sites within the DMC region. The model employs a one-
382 dimensional approach that does not explicitly account for lateral fluxes; however, this simplification is intentional.
383 It enables clearer interpretation of process-level dynamics under contrasting vegetation and climate conditions,

384 making it suitable for general scenario analysis. This assumption is especially justified in the DMC catchment,
 385 which is characterized by flat, lowland topography and is predominantly governed by vertical hydrological fluxes
 386 (Kleine et al., 2021; Smith et al., 2020).

387 The framework is not intended to reproduce exact spatial patterns or detailed species-specific physiology, but
 388 rather to capture the dominant effects of vegetation structure on vertical water fluxes and soil moisture dynamics.
 389 By focusing on variations in forest type, forest density, and root distribution associated with forest age and
 390 management, the framework enables a generalized assessment of long-term water partitioning and
 391 ecohydrological resilience under comparable environmental conditions. As such, it provides a practical and
 392 transferable tool for evaluating forest management impacts on water availability and ecohydrological resilience
 393 in drought-sensitive lowland catchments.



394

395 **Figure 3.** Matrix of nine Scenario Groups formed by combining three site-specific configurations (Broadleaf Site,
 396 Conifer Site, and Agroforest Site) with three forest types (Broadleaf, Conifer, and Agroforest). Each colored block
 397 represents a Scenario Group consisting of multiple sub-scenarios (e.g., varying forest densities and root water
 398 uptake distributions). Diagonal entries (Scenario Groups 1, 5, and 9), marked as “observed configuration”,
 399 correspond to forest–site combinations observed at the field sites, where vegetation type and site-specific soil–
 400 hydraulic and boundary conditions are consistent with real-world conditions.

401 4 Results

402 4.1 Dynamics of Soil Moisture and Soil Water Isotopes at the Broadleaf Forest Site

403 Figure 4 shows the 25-year baseline simulations of soil moisture and soil water isotopes dynamics at the broadleaf
 404 forest site at a daily time step as an example. In general, the model effectively captures the magnitude, variability,
 405 extremes, and timing of soil moisture dynamics. Surface soil moisture shows higher variability than deeper layers.
 406 Based on the modified Kling-Gupta Efficiency (mKGE), soil moisture simulations generally perform better in the
 407 deep layer than in the upper and middle layers, though this may partly reflect the more limited variance in deeper

408 soil moisture. In addition, the model slightly overestimates low soil moisture in the deeper layers during wet
 409 summers (e.g., 2023, 2024) and underestimates soil moisture during dry winters (e.g., 2021 and 2022). Soil water
 410 isotope simulations also perform well, with higher mKGE values in the middle layer than in upper and deep layers.
 411 The uncertainty range of soil water isotope simulations is narrower than that of soil moisture, indicating lower
 412 uncertainty in the isotope predictions.

413 Table 3 shows the modified Kling-Gupta Efficiency (mKGE) and Root Mean Square Error (RMSE) values for
 414 soil moisture and soil water isotopes across different land use plots. In all other cases the mKGEs for soil moisture
 415 are similar to the broadleaved plot, and soil water isotopes are reasonably reproduced, indicating the model's
 416 robustness and transferability. These results provide strong support for the appropriateness of applying EcoPlot-
 417 iso to assess the impacts of alternative forest management scenarios in subsequent analyses. In addition, simulated
 418 evapotranspiration was independently evaluated against MODIS-derived ET for all land use types, with model
 419 performance quantified using RMSE and mKGE metrics (Table S4). This independent evaluation provides further
 420 support for the model's ability to reproduce key water fluxes beyond the variables used for calibration.

421 **Table 3.** Model performance metrics for soil moisture and soil water isotopes ($\delta^2\text{H}$) at each land use site over the
 422 full evaluation period (2000–2024), evaluated using the modified Kling–Gupta Efficiency (mKGE) and the root
 423 mean square error (RMSE, mm for soil moisture and ‰ for $\delta^2\text{H}$). Metrics are computed by comparing observed
 424 and simulated time series at each soil depth.

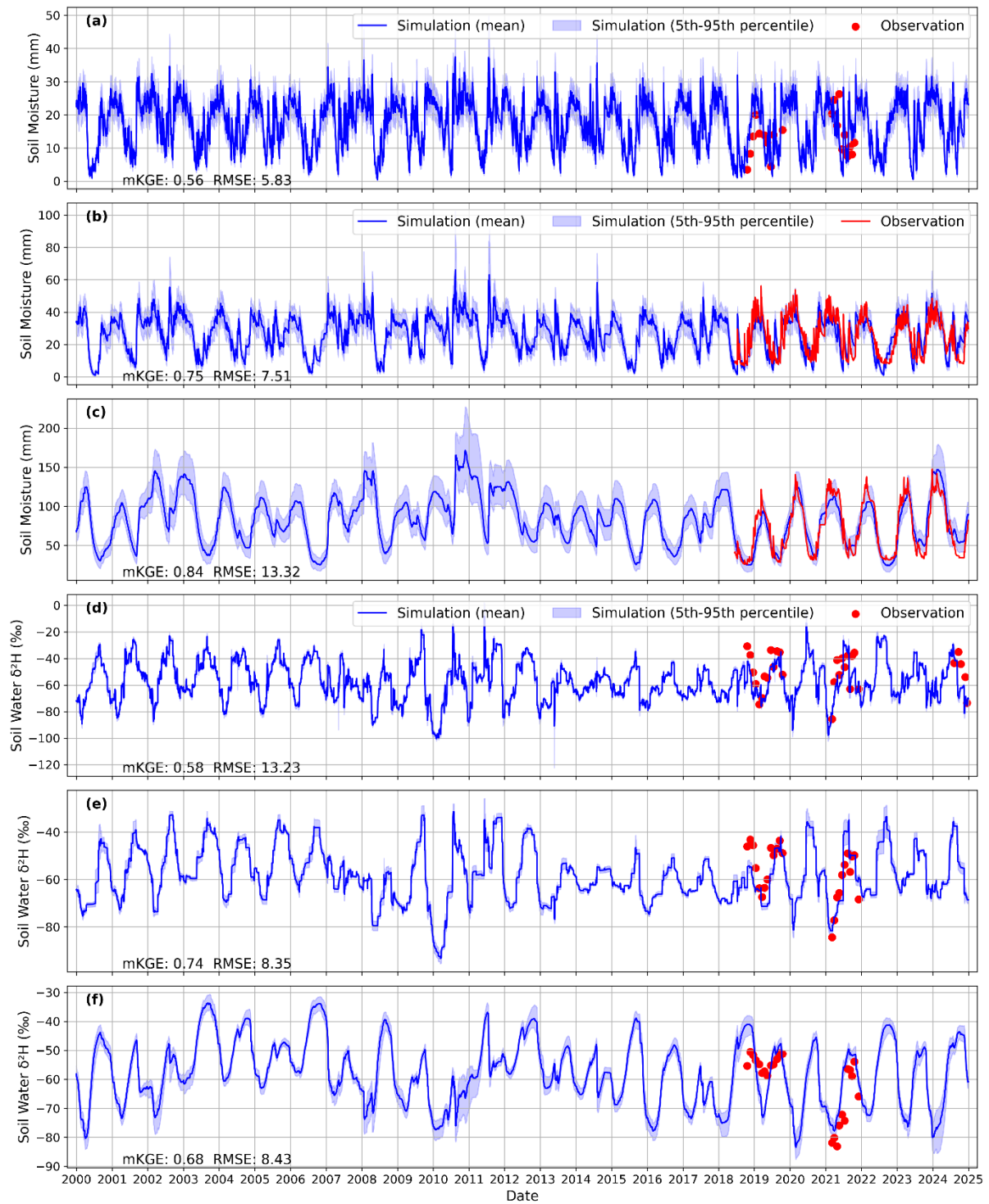
Sites	Soil moisture						Soil water isotope ($\delta^2\text{H}$)					
	Upper		Middle		Deep		Upper		Middle		Deep	
	mKGE	RMSE	mKGE	RMSE	mKGE	RMSE	mKGE	RMSE	mKGE	RMSE	mKGE	RMSE
Broadleaf Forest	0.56	5.83	0.75	7.51	0.84	13.32	0.58	13.23	0.74	8.35	0.68	8.43
Conifer forest	0.61	5.77	0.68	8.68	0.70	5.56	0.67	11.69	0.80	6.94	0.50	13.09
Agroforestry	0.72	5.22	0.79	6.63	0.77	23.43	0.82	8.09	0.85	10.45	0.79	8.98
Grassland	0.89	1.67	0.71	6.18	0.72	16.01	0.71	9.07	0.77	7.69	0.61	8.36
Cropland	0.53	5.84	0.62	8.88	0.71	22.36	0.83	8.36	0.85	9.19	0.36	13.71

425

426

427

428



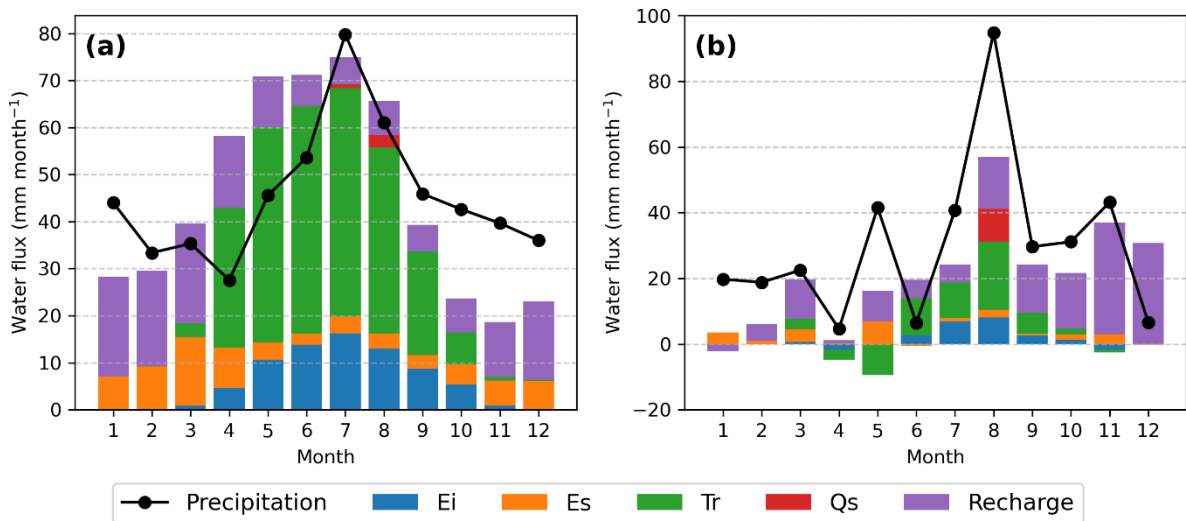
429
 430
 431
 432
 433
 434
 435
 436
 437

Figure 4. Long-term (2000–2024) simulations of soil moisture and soil water isotope ($\delta^2\text{H}$) at three different depths using EcoPlot-iso at a broadleaf forest site in the Demnitzer Millcreek catchment. (a–c) Simulated (mean \pm 5th–95th percentile) and observed soil moisture at upper (0–10 cm), middle (10–30 cm), and deep (30–100 cm) layers. (d–f) Simulated (mean \pm 5th–95th percentile) and observed soil water isotopic composition ($\delta^2\text{H}$) at corresponding depths. The blue line represents the mean value of the 100 best simulations, while the shaded area indicates the range between the 5th and 95th percentiles of these simulations. The red points and red line represent observed values. Modified Kling-Gupta Efficiency (mKGE) values for each simulation are indicated in the respective panels.

438 **4.2 Water Balance Components Under Different Wetness Conditions at the Broadleaf Forest Site**

439 Figure 5 presents the mean monthly water balance components and their changes between dry and wet years for
 440 the baseline simulation at the broadleaved forest site from 2000 to 2024. Groundwater recharge dominates blue
 441 water fluxes, while surface runoff is rare and occurs only during extreme summer rainfall events (Fig. 5a).
 442 Transpiration and canopy evaporation dominate in summer, while soil evaporation peaks in spring. Across dry
 443 and wet years, groundwater recharge shows the strongest sensitivity to interannual wetness, with reduced recharge
 444 during dry years and enhanced recharge during wet years following precipitation anomalies (Figs. 5b and S1). In
 445 contrast, transpiration remains relatively stable despite differences in annual wetness, indicating resilient
 446 vegetation function. This stability likely reflects the mature age of the forest (~60 years), although gradual changes
 447 in forest structure over the 20-year period may also play a role. Corresponding water balance results for the conifer
 448 forest and agroforestry sites are provided in the Supplementary Material (Fig. S9). Across the three forest types,
 449 the conifer forest exhibits the largest changes in groundwater recharge between dry and wet years, particularly in
 450 August, whereas agroforestry shows comparatively smaller changes than the broadleaf forest, indicating higher
 451 ecohydrological resilience. Overall, these seasonal patterns offer key insights into water partitioning under three
 452 forest baseline conditions and establish an important baseline for evaluating the impacts of alternative forest
 453 management scenarios.

454



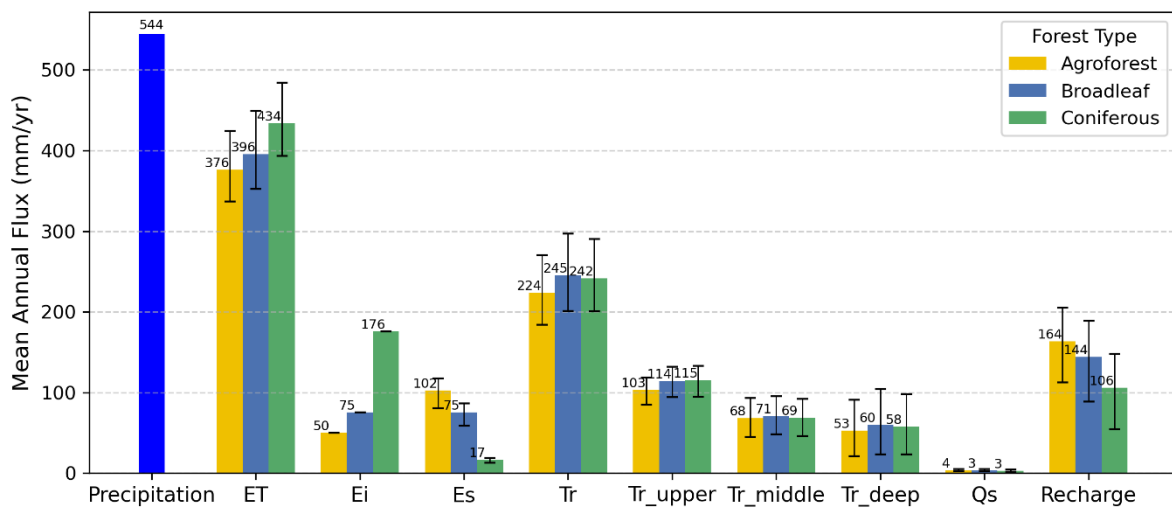
455 **Figure 5.** Mean monthly water balance components for the broadleaf forest site in the Demnitzer Millcreek
 456 catchment over 2000–2024, simulated with EcoPlot-iso using the mean of the best 100 parameter sets (see Section
 457 3.4 for details). Stacked bars show monthly totals of interception evaporation (Ei), soil evaporation (Es),
 458 transpiration (Tr), surface runoff (Qs), and groundwater recharge, while the black line indicates precipitation (P).
 459 (a) Long-term mean monthly water balance (mm month⁻¹). (b) Differences between wet years (2002, 2007, 2010,
 460 2023) and dry years (2006, 2018, 2022), expressed as wet minus dry (mm month⁻¹).
 461
 462

463 **4.3 Impacts of Forest Management on Water Partitioning and Soil Moisture**

464 Results in this section are based on the full forest management scenario framework, including all nine forest–site
 465 Scenario Groups and their associated ensemble simulations (Fig. 3), rather than on the observed baseline
 466 configurations alone.

467 **4.3.1 Water Balance and Partitioning Across Forest Types**

468 Figure 6 compares the mean annual water balance components across broadleaf forest, coniferous forest, and
 469 agroforestry types based on the ensemble mean of simulations derived from the paired vegetation–site soil
 470 parameter configurations (Fig. 3), under reference canopy and rooting conditions ($LAI\ scaling = 1; \beta = 1 \times \beta$).
 471 Results showed that evapotranspiration under coniferous forests accounted for 7% more of annual precipitation
 472 than broadleaf forest, and 11% more than in agroforestry systems. This was primarily due to higher transpiration
 473 (Tr) and canopy interception evaporation (Ei). Accordingly, soil evaporation (Es) and groundwater recharge
 474 ($Recharge$) were lowest in conifers and highest in agroforestry. Agroforestry had 11% more groundwater recharge
 475 relative to annual precipitation than conifers, and 4% more than broadleaf forests. Across forest types, the largest
 476 fraction of transpiration originated from the upper soil layer (Tr_upper), reflecting its closer coupling to
 477 precipitation inputs and higher soil moisture availability, while surface runoff (Qs) remained minimal and nearly
 478 identical. These results reflect the influence of forest structure and canopy cover on ecohydrological partitioning,
 479 with coniferous systems favoring atmospheric losses and agroforestry promoting soil evaporation and subsurface
 480 recharge. They underscore the trade-offs between evapotranspiration and groundwater recharge across different
 481 forest types.

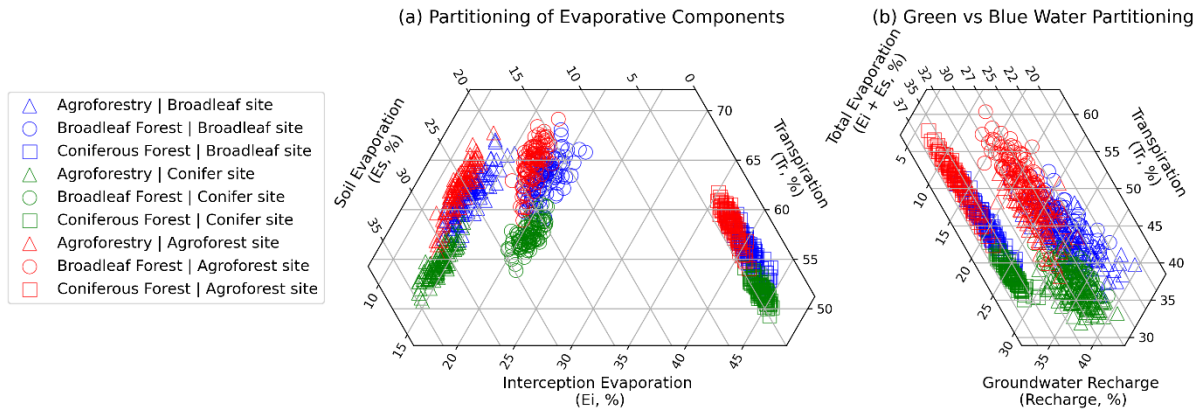


482 **Figure 6.** Comparison of mean annual water balance components across different forest types: broadleaf (blue),
 483 coniferous (green), and agroforestry (yellow). Bars represent the mean annual flux based on 25-year totals, with
 484 error bars indicating the 5th and 95th percentile ranges of the 100 best simulations. All simulations were conducted
 485 under baseline conditions with a fixed forest root parameter β of 0 and LAI scaling factor of 1.0.
 486

487 Figure 7 presents ternary diagrams illustrating the relative partitioning of key water flux components across three
 488 forest types based on individual simulations from the paired vegetation–site soil parameter configurations under
 489 reference canopy and rooting conditions. Transpiration predominates in all three forest types (Fig. 7a). The conifer
 490 forest exhibits a distinct pattern, characterized by the lowest soil evaporation (Es) and the highest interception
 491 evaporation (Ei) partitioning compared to broadleaf forest and agroforestry systems (Fig. 7a). In terms of green–
 492 blue water partitioning, the agroforestry system shows the largest groundwater recharge contribution (Fig. 7b).
 493 Figure 7b also highlights a clear trade-off between transpiration and groundwater recharge, reflecting both
 494 equifinality among the 100 best-performing parameter sets and differences in site-specific soil properties.
 495 Broadleaf and agroforestry forests display largely overlapping partitioning patterns overall, although interception
 496 evaporation and total evaporation differ notably between the two (Fig. 7a–b). Differences in soil properties also

497 influence transpiration partitioning, following the order agroforestry site > broadleaf site > conifer site. The
 498 conifer site is characterized by coarse sandy soil with lower water retention and faster drainage, whereas the
 499 agroforestry site has greater water-holding capacity, which likely contributes to the observed differences in
 500 transpiration.

501



502 **Figure 7.** Water flux partitioning illustrated using ternary diagrams based on the 100 best model simulations
 503 derived from the paired vegetation–site soil parameter configurations for three forest types: agroforestry, broadleaf
 504 forest, and coniferous forest, under reference canopy and rooting conditions (LAI scaling = 1.0; $\beta = 1 \times \beta$). (a)
 505 Partitioning of total evapotranspiration into transpiration (Tr), soil evaporation (Es), and interception evaporation
 506 (Ei). (b) Partitioning of water fluxes into green water (Tr and $E = Ei + Es$) and blue water (groundwater recharge).
 507 Each point represents the normalized annual mean flux from a 25-year simulation. Colored markers denote
 508 different forest types.
 509

510 4.3.2 Annual Mean Water Flux Responses to Forest Management Scenarios

511 The annual mean responses of key ecohydrological fluxes to forest management scenarios across all paired
 512 vegetation–site configurations are summarized in Fig. 8, while the detailed number and visualization of green and
 513 blue water partitioning are provided in the Fig. S10 in Supplementary Material. Figure S10 presents heatmaps of
 514 evapotranspiration (ET), groundwater recharge (Recharge), transpiration (Tr), ET partitioning (ET/P),
 515 groundwater recharge partitioning (Recharge/P) and green water partitioning (Tr/ET) for agroforests, broadleaf
 516 forest, and coniferous forest scenarios.

517 Across all forest management scenarios, annual mean evapotranspiration ranges from 285 mm/yr to 454 mm/yr,
 518 with ET fraction relative to precipitation varying between 0.52 and 0.84 (Fig. S10). In contrast, groundwater
 519 recharge ranges from 85 mm/yr to 254 mm/yr, reflecting strong sensitivity to vegetation structure and canopy
 520 density. Annual mean transpiration (Tr) varies between 77 mm/yr and 261 mm/yr, with the corresponding green
 521 water partitioning (Tr/ET) ranging from 0.27 to 0.64. These results underscore the significant influence of
 522 vegetation type and structure on ecohydrological fluxes and water partitioning outcomes.

523 Consistent with these detailed patterns, Figure 8 shows that both transpiration and evapotranspiration increase
 524 with higher LAI scaling factors, while groundwater recharge decreases. Figures 8a and 8b illustrate the trade-off
 525 between increased ET and reduced groundwater recharge under different forest management scenarios. ET and
 526 transpiration rise rapidly at first, then slow down and transpiration even slightly decreases for conifer forests due
 527 to increased interception evaporation and soil moisture limitation (Figs. 8c and 8i). This decline is not observed
 528 in broadleaf or agroforestry systems, likely due to their different seasonal LAI patterns. While summer LAI values

529 for broadleaf and coniferous forests may be similar, the consistently high year-round LAI in conifers can
530 exacerbate moisture stress.

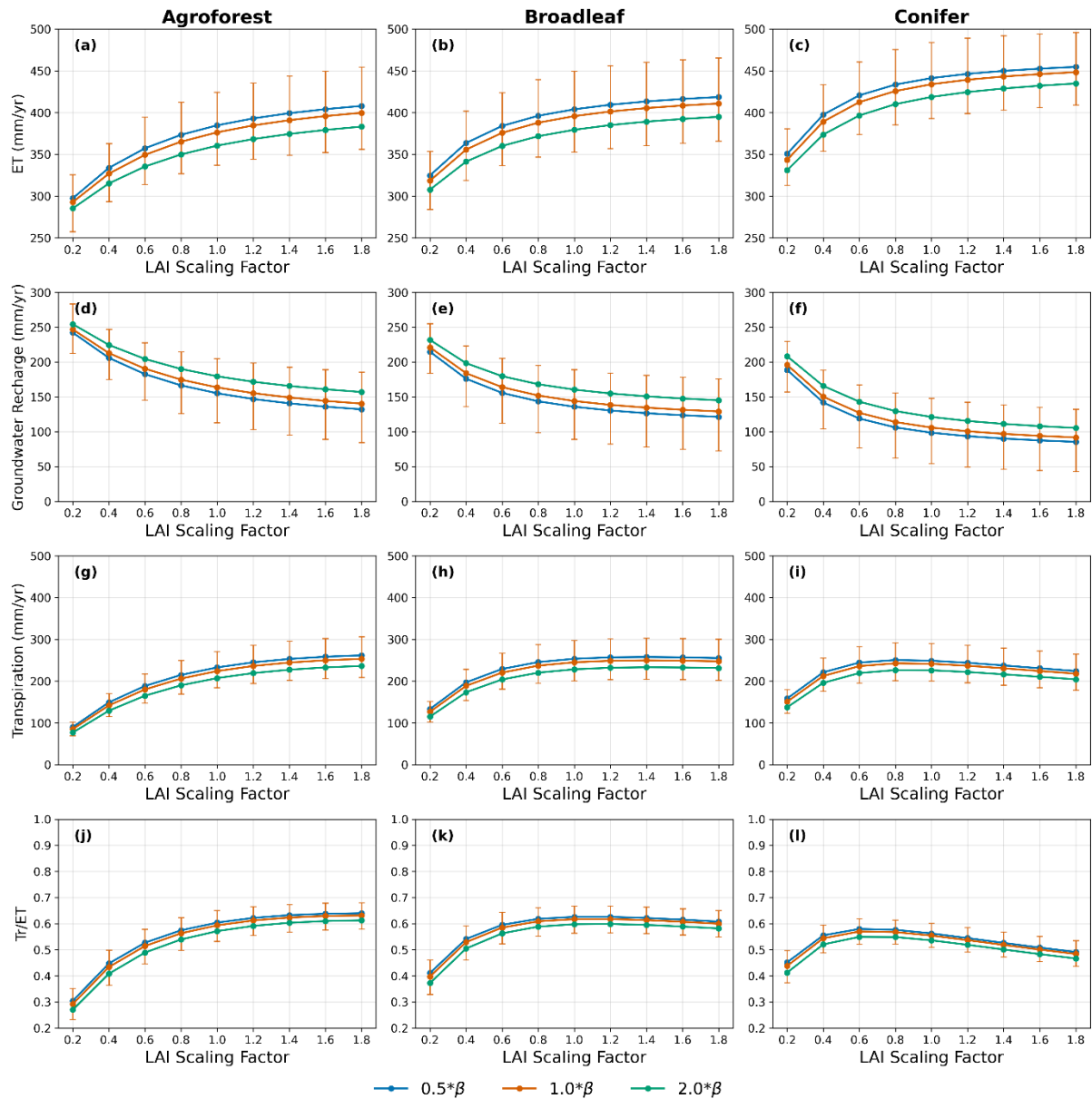
531 At higher LAI levels, transpiration decreases slightly while canopy interception evaporation increases (Fig. S11).
532 In dense coniferous stands, excessive interception and persistently dry soils limit root water uptake, reducing
533 vegetation function. This highlights a trade-off between transpiration and interception evaporation. The resulting
534 moisture limitation suggests that such high-density forests may not be sustainable under water-limited conditions,
535 as this negative feedback could constrain long-term forest growth and persistence. In addition, forests with
536 shallow-rooted trees—such as young stands —tend to transpire less, generate more groundwater recharge, and
537 exhibit lower Tr/ET ratios compared to deep-rooted forests. However, under high canopy density conditions,
538 transpiration declines across rooting scenarios, suggesting that this reduction is driven not only by soil moisture
539 limitation, but also by increased interception evaporation.

540

541

542

543



544
 545 **Figure 8.** Annual mean ecohydrological fluxes for three forest types (Agroforest, Broadleaf, and Conifer) under
 546 varying LAI scaling factors and root depth scenarios, based on the ensemble mean of simulations derived from
 547 the paired vegetation–site soil parameter configurations (Figure 3). Panels (a)–(c) show evapotranspiration (ET),
 548 (d)–(f) show groundwater recharge, (g)–(i) show transpiration, and (j)–(l) show the ratio of transpiration to total
 549 evapotranspiration (Tr/ET). Lines represent different rooting depth scenarios (β), while vertical bars denote the
 550 5th–95th percentile range across ensemble simulations for the baseline rooting scenario ($\beta = 1 \times \beta$).

551 **4.3.3 Monthly Dynamics of Water Fluxes Responses to Forest Management Scenarios**

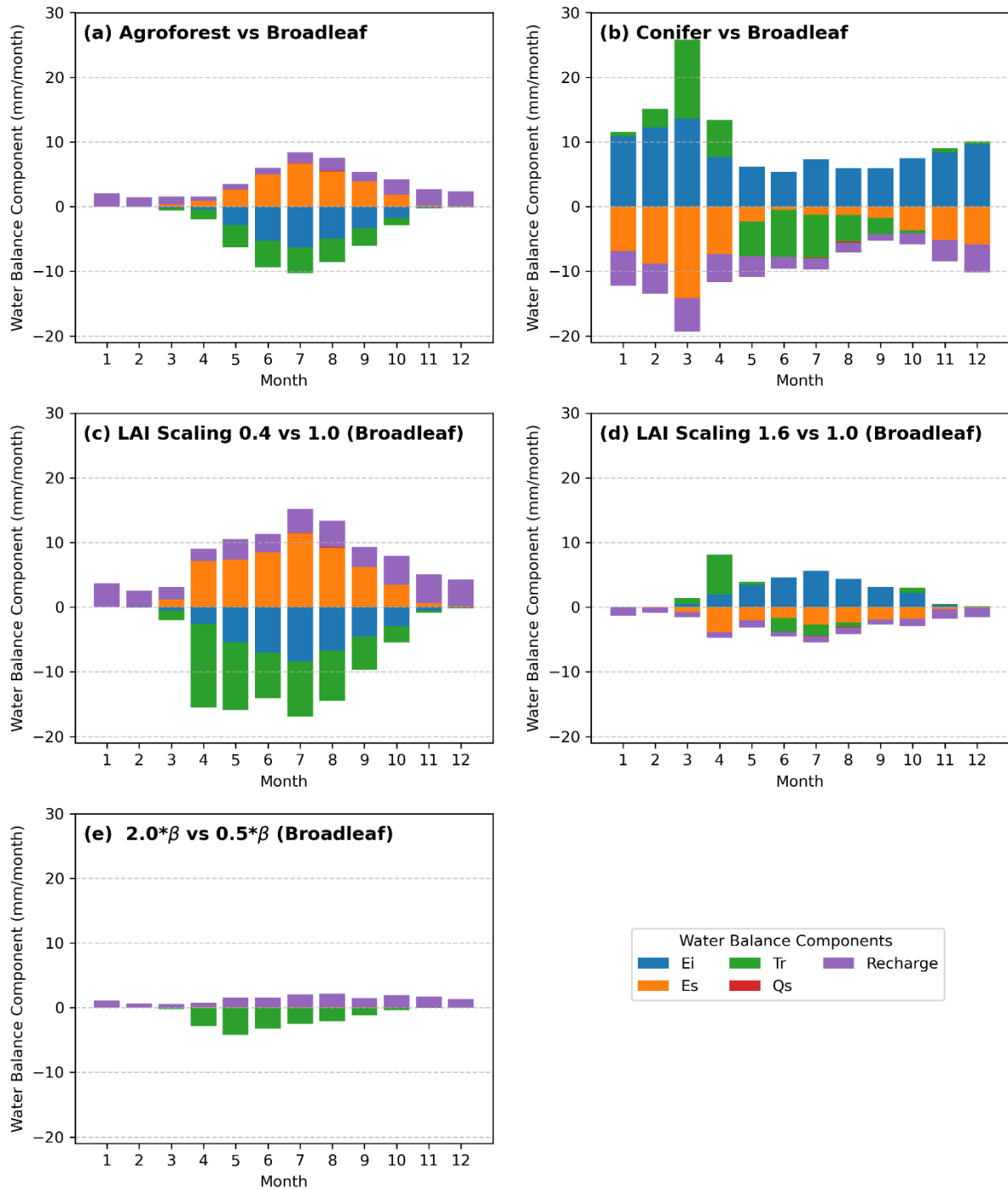
552 Figure 9 shows monthly deviations in water balance components across forest management scenarios, based on
 553 the ensemble mean of simulations derived from the paired vegetation–site soil parameter configurations (Fig. 3)
 554 under reference canopy and rooting conditions (LAI scaling = 1; $\beta = 1 \times \beta$). Relative differences among forest
 555 types indicate that agroforestry exhibits lower transpiration and canopy evaporation, but higher soil evaporation
 556 during summer compared to broadleaf forests (Fig. 9a). They are also associated with greater groundwater
 557 recharge from summer through the following winter. A shift from broadleaf to conifer forests is expected to have
 558 a greater impact on the water balance than the shift from agroforest to broadleaf (Fig. 9a and 9b). Compared to
 559 broadleaf forests, conifer forests exhibit higher simulated transpiration in March (Fig. 9b), driven by increased

560 potential evapotranspiration and a relatively higher leaf area index (LAI) under wet soil conditions. This difference
561 diminishes as the LAI of broadleaf forests increases in spring.

562 Changes in the LAI scaling factor influence water balance components in summer, increasing transpiration and
563 canopy evaporation while reducing recharge and soil evaporation (Fig. 9c and 9d). Increasing the LAI scaling
564 factor from 0.4 to 1.0 has a greater impact than reducing it from 1.6 to 1.0, as vegetation water use responds more
565 sensitively at low LAI values but plateaus at higher values due to energy or soil moisture limitations. Altering the
566 forest root parameter (β), while using the same LAI time series, primarily affects deep-layer transpiration,
567 reducing total transpiration and increasing recharge. Other water balance components remain unchanged because
568 the LAI time series is held constant.

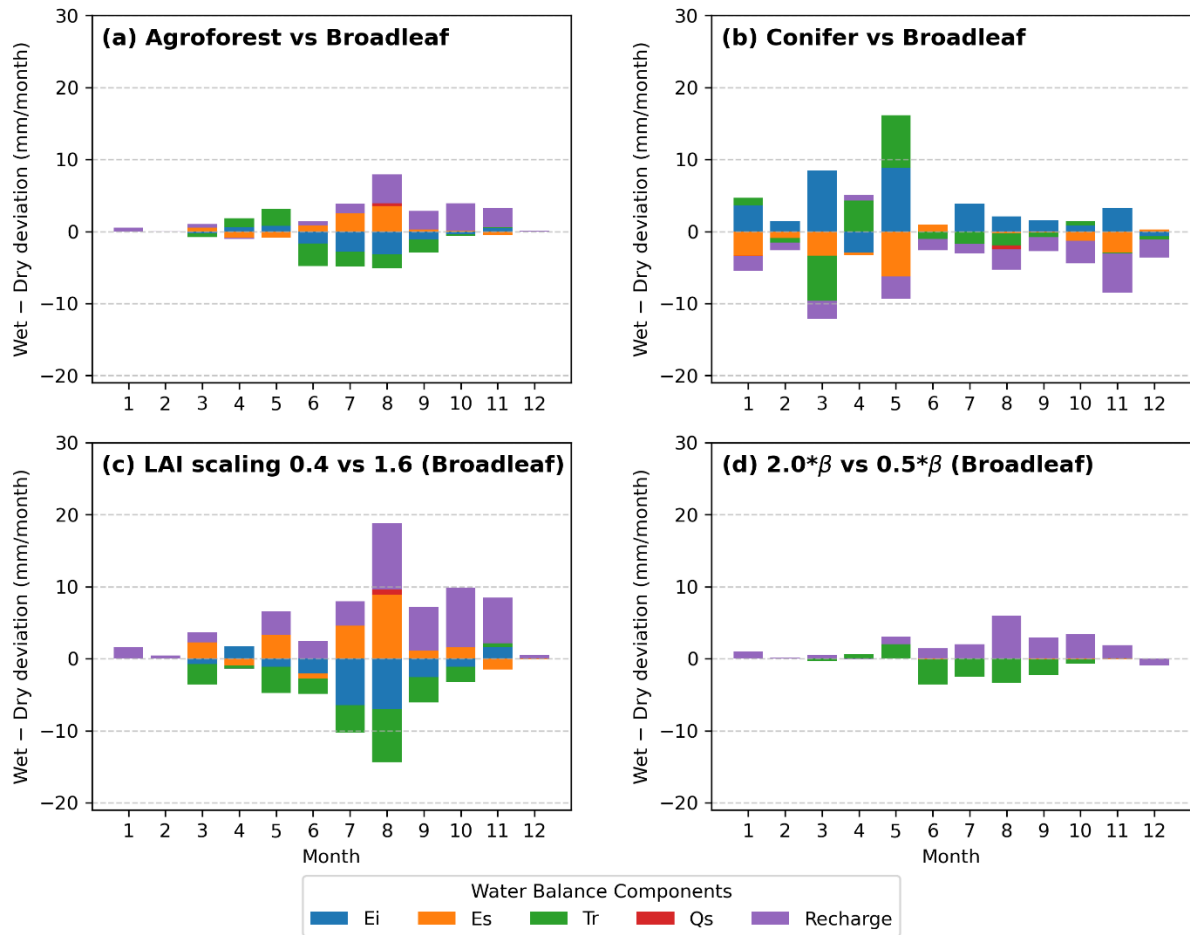
569 Figure 10 extends the monthly analysis by explicitly comparing wet–dry-year differences in water balance
570 responses across forest type, canopy density, and rooting scenarios. In contrast to Figure 9, which presents mean
571 monthly deviations relative to reference conditions, and Figure 5b, which shows the baseline wet–dry-year
572 differences, Figure 10 highlights how these wet–dry contrasts vary among scenarios, thereby isolating drought-
573 sensitivity effects.

574 For agroforestry relative to broadleaf forests, hydroclimatic contrasts primarily affect groundwater recharge and
575 transpiration, with the largest wet–dry differences occurring in late summer (Fig. 10a). This indicates a more
576 buffered late-summer transpiration response in agroforestry systems under drought conditions. In contrast,
577 differences between coniferous and broadleaf forests show the largest wet–dry contrasts in transpiration during
578 May (Fig. 10b), rather than March as indicated by the mean monthly deviations in Figure 9b. This seasonal shift
579 indicates that conifer transpiration is most drought-sensitive during the later spring period, likely reflecting
580 sustained year-round transpiration and associated soil moisture drawdown in conifer forests, and highlighting
581 differences in early growing-season water-use strategies between coniferous and broadleaf forests. Figures 10c
582 and 10d show that wet–dry differences are largest in summer (August), indicating that drought conditions amplify
583 ecohydrological differences between low and high canopy density, as well as between shallow and deep rooting
584 scenarios, particularly for transpiration and groundwater recharge. Overall, Figure 10 demonstrates that
585 hydroclimatic extremes not only modify the magnitude of vegetation controls on water partitioning but also shift
586 their seasonal expression, with important implications for ecohydrological resilience under future drought
587 conditions.



588 **Figure 9.** Monthly deviations of water balance components relative to the baseline broadleaf forest scenario, based
 589 on the ensemble mean of simulations derived from the paired vegetation–site soil parameter configurations (Fig.
 590 3) under reference canopy and rooting conditions (LAI scaling = 1; $\beta = 1 \times \beta$). Each panel illustrates the deviation
 591 of monthly water balance components from the baseline simulation, with only one parameter modified in each
 592 scenario: (a) Agroforest, (b) Conifer forest, (c) LAI scaling factor = 0.4, (d) LAI scaling factor = 1.6, and (e) Root
 593 parameter $\beta = 2.0$. Tr: transpiration, Ei: canopy evaporation, Es: soil evaporation, Qs: surface runoff, Recharge:
 594 groundwater recharge.
 595

596



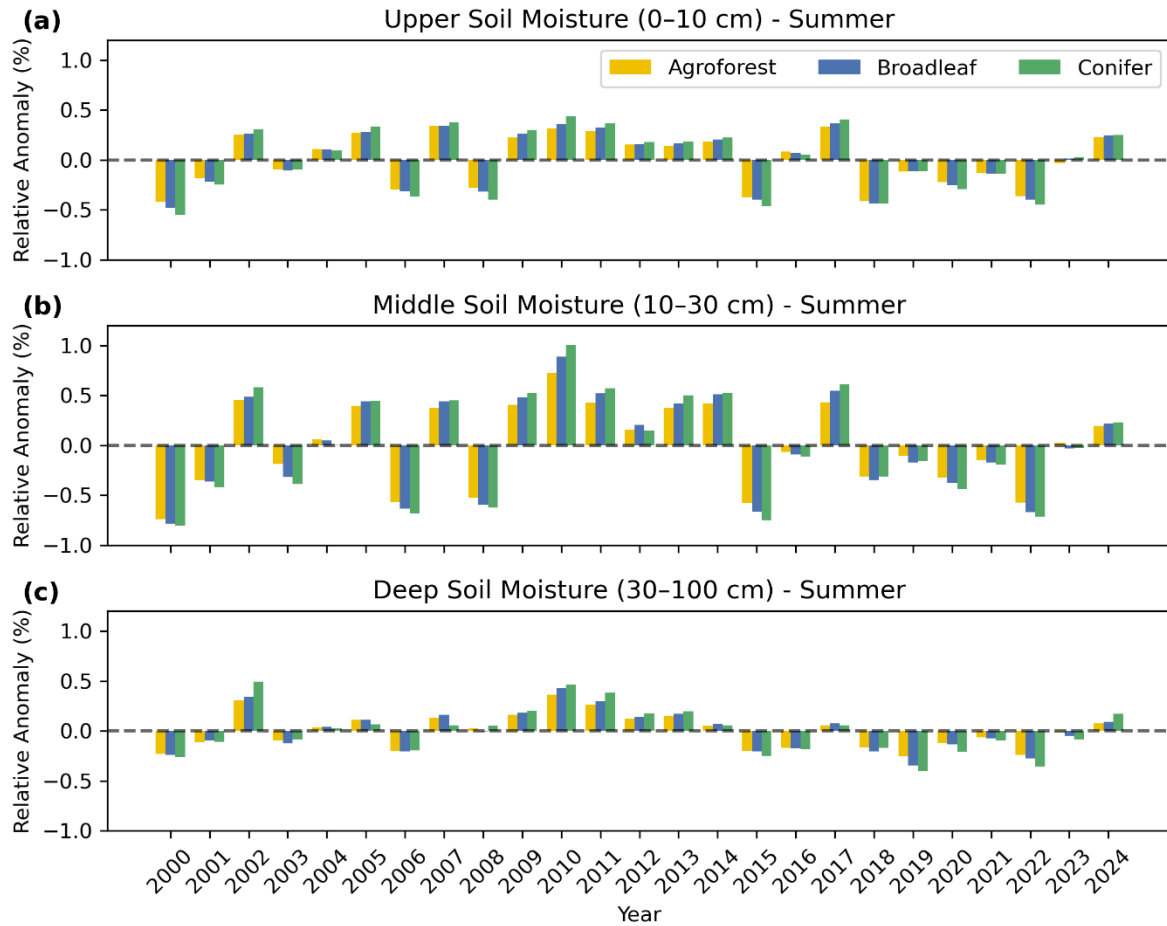
597

598 **Figure 10.** Monthly differences in water balance component deviations between wet and dry years across forest type, LAI scaling, and rooting (β) scenarios. For each panel, values show the difference between wet-year and dry-year deviations of a given scenario relative to its reference scenario; positive (negative) values indicate stronger (weaker) contributions during wet years. Panels show: (a) Agroforest vs. Broadleaf; (b) Conifer vs. Broadleaf; (c) LAI scaling 0.4 vs. 1.6 for Broadleaf; (e) $2.0 \times \beta$ vs. $0.5 \times \beta$ for Broadleaf. Stacked bars indicate contributions from interception evaporation (E_i), soil evaporation (E_s), transpiration (T_r), surface runoff (Q_s), and groundwater recharge (Recharge). Wet years are 2002, 2007, 2010, and 2023; dry years are 2006, 2018, and 2022.

605 4.3.4 Soil Moisture Anomalies

606 Figure 11 shows the relative summer soil moisture anomalies across three forest types and three soil layers. Anomalies are calculated as the percentage deviation from the long-term seasonal mean, enabling normalized comparison across forest types and soil layers. Conifer forests exhibit the strongest soil moisture anomalies, followed by broadleaf forests, while agroforests exhibit the least variability, indicating greater stability in soil moisture. Furthermore, among the three soil layers, the middle layer (10–30 cm) consistently shows stronger anomalies across all forest types, with magnitudes nearly double those of the other layers, highlighting its vulnerability during summer drought. In contrast, the upper layer (0–10 cm) and deep layer (30–100 cm) exhibit weaker anomalies, likely due to frequent soil moisture replenishment by summer rainfall in the upper layer and either more stable moisture retention or greater water storage capacity at depth that compensates for drought impacts. Negative soil moisture anomalies are more pronounced in summer than in spring, reflecting the stronger seasonal drought effects and fluctuations in soil moisture (see Fig. S12). During spring, broadleaf forests and

617 agroforests display similar negative soil moisture anomalies, suggesting comparable seasonal soil moisture
 618 dynamics between these forest types.



619
 620 **Figure 11.** Relative summer (June–August) soil moisture anomalies across three soil layers: (a) upper (0–10 cm),
 621 (b) middle layer (10–30 cm), and (c) deep layer (30–100 cm) for three forest types (Agroforest, Broadleaf,
 622 Conifer). Results are based on the ensemble mean of simulations derived from the paired vegetation–site soil
 623 parameter configurations (Fig. 3) under reference canopy and rooting conditions (LAI scaling = 1; $\beta = 1 \times \beta$).
 624 Bars represent deviations from the long-term mean, with positive values indicating wetter conditions and negative
 625 values indicating drier conditions.

626 **5 Discussion**

627 **5.1 Vegetation Controls on Water Partitioning under Contrasting Forest Management Scenarios**

628 Assessing the influence of different land use types on water availability is inherently challenging because of the
 629 complex interactions among vegetation, climate, and soil properties (te Wierik et al., 2021; Zhang et al., 2001).
 630 Different vegetation types have distinct water demands, and their contrasting canopy structures affect how
 631 precipitation is intercepted and partitioned into infiltration, runoff, groundwater recharge, and evapotranspiration
 632 (Brauman et al., 2010). Vegetation management practices can substantially alter these processes. Moreover, the
 633 effects of vegetation and canopy structure may vary depending on underlying soil characteristics (Geris et al.,
 634 2015). This complexity poses a significant challenge for land managers and policymakers, particularly in drought-
 635 sensitive regions experiencing increasing aridity under climate change (Orth and Destouni, 2018). In such contexts,

636 providing informed guidance on sustainable land cover choices is increasingly important for maintaining long-
637 term water availability (Estrela and Vargas, 2012). In regions where forestry has traditionally been a dominant
638 land use, shifting hydroclimatic conditions underscore the need to assess how different forest types and
639 management practices affect water partitioning and drought vulnerability (Quandt et al., 2023). This requires
640 evaluating water yield across multiple temporal scales, including the effects of forest management on annual and
641 monthly water partitioning, and their implications for residual water availability—specifically streamflow
642 generation and groundwater recharge during low-flow periods (Brown et al., 2005; Neill et al., 2021).

643 Although complex, process-based ecohydrological models such as RHESSys and EcH₂O are well suited to
644 capturing detailed interactions among hydrological processes and water fluxes in data-rich research settings, their
645 broader application in forest and land management is often constrained by the availability of observation data
646 required for model forcing and calibration, as well as computational demand (Fatichi et al., 2012; Kuppel et al.,
647 2018; Tague and Band, 2004). In this study, we therefore adopt a parsimonious, tracer-aided, conceptual process-
648 based modelling approach. This was not to replace more complex models, but to provide robust and management-
649 relevant insights into the dominant vegetation-structural controls governing water partitioning under different
650 forest management scenarios. This focus is particularly relevant for Brandenburg, northeastern Germany, where
651 recent droughts have highlighted the vulnerability of traditional forest management practices dominated by Scots
652 pine plantations (Luo et al., 2024). By employing the tracer-aided ecohydrological model EcoPlot-iso, we
653 developed and applied a generic framework to quantify the long-term effects of variations in forest type, forest
654 density and root distribution on both blue and green water fluxes. The framework is based on idealized
655 monoculture forest scenarios and explicitly acknowledges that additional species-specific and process-level
656 dynamics (e.g., stomatal regulation, VPD sensitivity, drought stress strategies) are not represented and remain
657 important directions for future model development. While this study focused on idealized, homogeneous
658 vegetation scenarios (broadleaf and conifer) for clarity and comparability, mixed crop–tree systems such as
659 agroforestry could only be represented implicitly in EcoPlot-iso through aggregated plot-scale vegetation
660 parameters. Species-specific interactions and sub-grid vegetation heterogeneity are therefore not explicitly
661 resolved. The applied LAI scaling range represents an intentionally broad, management-relevant envelope for
662 exploring canopy density effects, and scenario results should therefore be interpreted in a relative rather than
663 prescriptive sense.

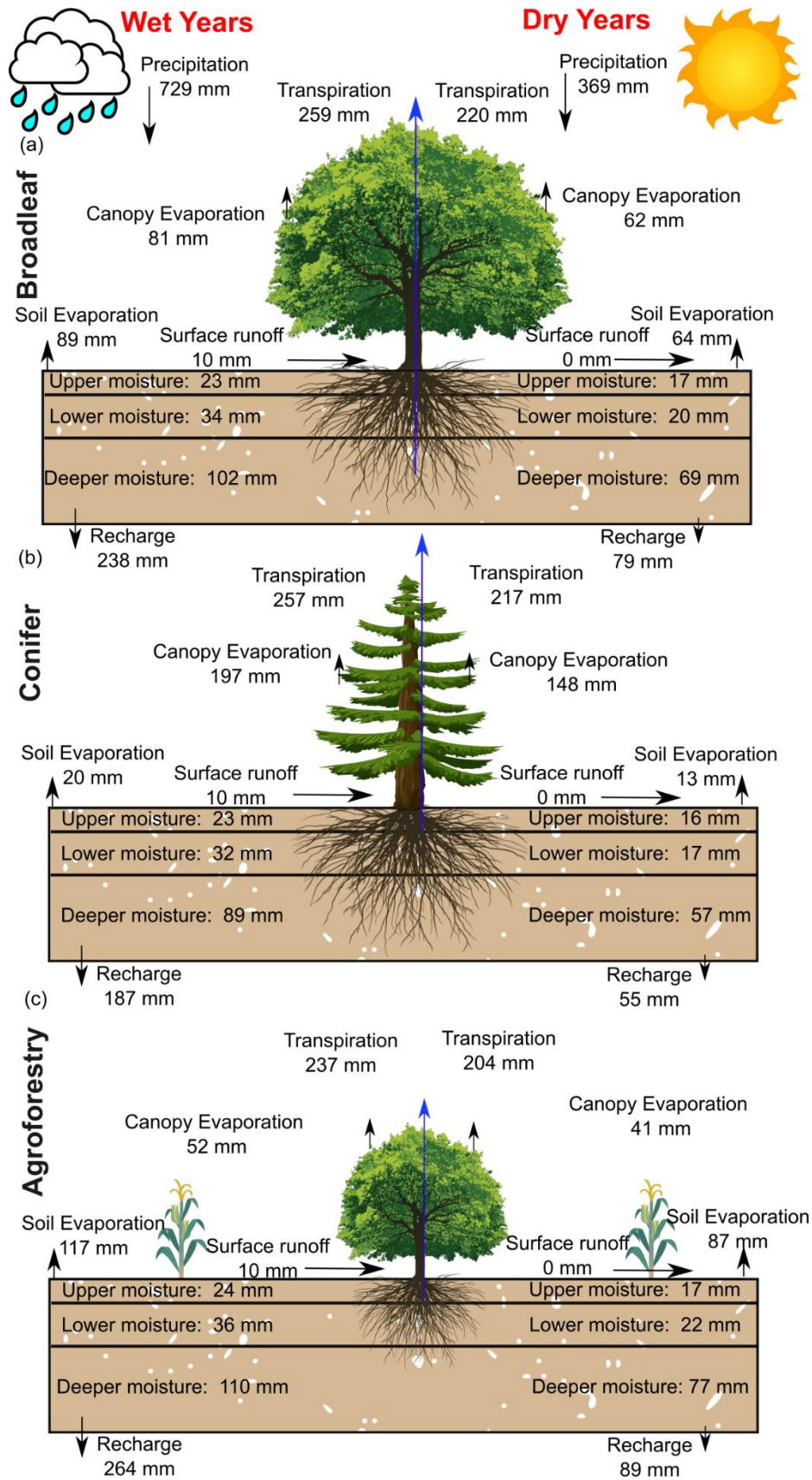
664 We acknowledge that the calibration of EcoPlot-iso is subject to parameter equifinality, whereby multiple
665 parameter combinations can reproduce the observed soil moisture and isotope dynamics with similarly good
666 performance. Rather than seeking a single optimal parameter set, our calibration strategy explicitly accounts for
667 this equifinality by propagating uncertainty from the 100 best-performing simulations into all key results. The
668 scenario framework further assumes that vegetation- and soil-related parameter sets can be recombined for
669 comparative scenario analysis, without explicitly preserving parameter correlations among the calibrated
670 ensembles. This may contribute to uncertainty inflation in some flux estimates and should therefore be considered
671 when interpreting the prediction intervals. Uncertainty envelopes (5th–95th percentiles) shown in Figures 4, 6,
672 and 8 illustrate the range of annual and seasonal flux responses, enabling the magnitude of parametric uncertainty
673 to be evaluated relative to differences among forest types and management scenarios. Although parametric
674 uncertainty is non-negligible and in some cases comparable to different forest management scenarios, the main
675 findings are supported by consistent ensemble-mean responses and clear directional differences in water

676 partitioning across scenarios. Accordingly, results are interpreted in a relative and comparative sense, emphasizing
677 management-relevant trade-offs rather than absolute flux predictions.

678 In the baseline simulations for broadleaf forest, conifer forest and agroforestry at the DMC site, the estimated
679 mean annual evapotranspiration (ET) over 2000–2024 was 396, 434, and 376 mm yr⁻¹, respectively, accounting
680 for approximately 73%, 80%, and 69% of annual precipitation. These values are consistent with previous
681 modelling studies at the DMC, which reported ET fractions ranging from 68% to over 80% of annual precipitation
682 (Smith et al., 2021; Landgraf et al., 2023). Differences among studies may reflect interannual climate variability
683 and the influence of particularly dry or wet years that are not captured by short-term assessments. Differences in
684 model structure, parameterization, and input data may also contribute to the spread in reported ET values. In
685 addition, to further assess model performance using an independent data source, simulated ET was evaluated
686 against MODIS-derived ET for all land use sites in the DMC, including broadleaf forest, conifer forest,
687 agroforestry, cropland, and grassland (Fig. S8 and Table S4). Model performance was quantified using mKGE
688 metrics calculated from daily ET, providing an external validation independent of the calibration data. While
689 EcoPlot-iso tends to slightly underestimate ET relative to MODIS observations, mKGE values indicate good
690 agreement in temporal dynamics across land-use types, supporting the model’s ability to reproduce key ET
691 variability. Overall, this evaluation underscores the importance of long-term simulations and independent data-
692 based validation for capturing representative ecohydrological behavior and for assessing the impacts of forest
693 management strategies under variable climatic conditions.

694 In catchments like DMC, where evapotranspiration (ET) is high, atmospheric demand is the primary driver of root
695 water uptake, though vegetation plays a key role in regulating its impact on water availability. In Brandenburg,
696 coniferous forests have traditionally been favored on sandy soils, but modelling indicates high water use due to
697 interception losses and year-round transpiration potential (Fig. S9c). Consequently, the implications for both
698 reduced groundwater recharge and reduced forest productivity have encouraged landowners to explore alternative
699 land use, such as broadleaf forests and agroforestry. These options have the potential to optimize biomass
700 productivity while enhancing landscape water retention, groundwater recharge, and drought adaptation.

701 These results (e.g., Figs. 8 and S10) have practical applications, such as estimating the direction and magnitude
702 of the changes in evapotranspiration and water yield as a function of forest management practices, driven by
703 alterations in canopy structure and rooting depth. The modelling approach thus provides useful insights into the
704 hydrological implications of alternative canopy structures and rooting patterns for water use. Figure 12 compares
705 the mean annual partitioning of water fluxes and soil moisture across broadleaf, coniferous, and agroforest types
706 under dry and wet year conditions. It highlights how different vegetation strategies influence ecohydrological
707 resilience, with substantial differences in water partitioning observed between dry and wet years across contrasting
708 forest management scenarios. By simulating long-term water availability across alternating wet and dry years,
709 EcoPlot-iso simulations suggest that agroforestry can support water availability in drought-sensitive catchments
710 by sustaining groundwater recharge as the dominant blue-water flux.



711

712 **Figure 12.** Comparison of mean annual water fluxes and soil moisture in the upper, middle, and deep layers for
 713 Broadleaf (a), Coniferous (b), and Agroforest (c) forests under dry (2006, 2018, 2022) and wet (2002, 2007,
 714 2010, 2023) year conditions.

715 **5.2 Soil Moisture Dynamics and Root Water Uptake Processes across Forest Management Scenarios**

716 At most of the monitoring plots in the DMC, groundwater is typically more than 3 meters below the ground surface
717 (Ying et al., 2025). Therefore, except in older forest plots with deeply rooting trees, vegetation relies on soil
718 moisture for root water uptake. Even for mature trees, there is evidence that most root water uptake occurs in the
719 near-surface soil horizons, as demonstrated by Birkel et al. (2025), 20 km from the DMC. A global synthesis by
720 Evaristo & McDonnell (2017) further supports this, indicating that ~77% of plant water uptake comes from
721 shallow sources, with deeper groundwater use primarily in more arid regions. While hydraulic redistribution may
722 provide deeper access for some species (Emerman and Dawson, 1996), rooting strategies are complex and highly
723 species-specific (Demir et al., 2024). In this context, our results highlight the middle soil layer (10–30 cm) as the
724 most reactive and significant for sustaining transpiration, with anomaly magnitudes nearly twice those of both the
725 upper (0–10 cm) and deep (30–60 cm) layers across all forest types.

726 In addition, seasonal comparisons revealed that summer soil moisture anomalies were more negative than those
727 in spring for all forest types (Fig. S12). This is likely linked to higher temperatures and evapotranspiration during
728 summer, which intensify water stress and drive seasonal variation in soil moisture availability. Forest density and
729 rooting characteristics substantially influenced the relative magnitude of soil moisture anomalies (Figs. S13 and
730 S14, respectively). Denser forests exhibited stronger negative anomalies during dry periods and enhanced positive
731 anomalies in wet periods, amplifying seasonal fluctuations. For example, high-density (LAI scaling factor 1.6)
732 conifer stands showed relative anomalies up to 25% greater than their low-density counterparts (Fig. S14). In
733 contrast, shallow-rooted systems moderated this response, leading to more stable soil moisture dynamics. Among
734 the management scenarios, agroforestry consistently exhibited the smallest anomalies, reflecting greater buffering
735 capacity and higher ecohydrological resilience.

736 The improved rooting scheme in EcoPlot-iso represents depth-dependent transpiration by dynamically linking
737 root water uptake efficiency to soil moisture availability across three soil compartments (see Section 3.2). The
738 implemented formulation enables transpiration demand to be partitioned across soil layers according to rooting
739 distribution and soil moisture availability within a parsimonious conceptual framework. The aim was not to
740 optimize species-specific root dynamics, but to represent the relative influence of rooting depth on water uptake
741 and partitioning, particularly in shallow-rooted or structurally diverse systems such as young forests. While the
742 new implementation improves the process representation of root–soil interactions, it did not result in a substantial
743 improvement in simulated soil moisture. For shallow vegetation types such as grasslands and croplands, model
744 performance—measured using the mKGE was similar with and without the new transpiration function (results
745 not shown). Moreover, direct validation of the root uptake scheme remains challenging due to the lack of
746 supporting observations, such as root distribution data, xylem water isotopes, or sap flux measurements.
747 Addressing this issue is a clear priority for future research.

748 These findings highlight how structurally diverse systems, such as agroforests, can buffer drought impacts by
749 improving groundwater recharge and reducing the amplitude of soil moisture fluctuations (Tetzlaff et al., 2024).
750 Together, these insights underscore the importance of rooting depth, forest structure, and seasonal climate
751 variability in shaping soil moisture patterns and regulating vegetation water use. Accounting for these factors is
752 essential for informing adaptive forest management in drought-sensitive catchments like the DMC.

753 **5.3 Advancing Tracer-Aided Ecohydrological Modelling: Challenges and Future Outlook**

754 This study demonstrates that tracer-aided ecohydrological models, such as the isotope-aided EcoPlot-iso, can be
755 used to effectively quantify the impact of forest management scenarios on water partitioning and ecohydrological
756 resilience. By distinguishing between evaporation, transpiration, and subsurface water movements using stable
757 isotopes (Soulsby et al., 2015), the model captures key hydrological responses—including evapotranspiration
758 (ET), groundwater recharge, and soil moisture dynamics—under varying management strategies. These insights
759 support evidence-based decision-making in drought-sensitive landscapes.

760 Despite these advances, several challenges remain. Conducted in a 66 km² mid-sized basin, this study did not
761 include land use change induced atmospheric feedbacks—such as changes in albedo, radiative balance, or rainfall
762 patterns—which are less critical at this scale but become important in larger-scale modeling (Ellison et al., 2012;
763 Filoso et al., 2017). Moreover, this study applied a multi-objective calibration approach, combined with Monte
764 Carlo sampling, that equally weighted isotopic and soil moisture data. However, further investigation is needed
765 into how these observational constraints are balanced and interpreted. Recent advances—such as the
766 DREAM(LoAX) framework (Wu et al., 2025)—demonstrate how simultaneous calibration and diagnostic
767 analysis under the equifinality thesis can improve parameter identifiability, model robustness, and process
768 understanding in tracer-aided ecohydrological models.

769 While this study used $\delta^2\text{H}$ to constrain evaporative fractionation given, the combined use of $\delta^{18}\text{O}$ and $\delta^2\text{H}$ (or d-
770 excess) may help improve the separation of evaporation effects and mixing processes (e.g. Penna et al., 2018)
771 though this was beyond the scope of this paper. Many recent studies have used isotopic data to investigate root
772 water uptake patterns, revealing how tree species, soil properties, and spatial water availability shape plant water
773 use strategies (Demir et al., 2024; Rothfuss and Javaux, 2017). Integrating tracer-aided models with soil and xylem
774 water isotope data offers a promising path to improving the representation of root water uptake, which is often
775 simplified in current modelling approaches (Birkel et al., 2025). Improving root uptake representation requires
776 consideration of species-specific traits and local soil-water conditions. However, the practical application of such
777 improvements is limited by the scarcity of soil and xylem water isotope data, which are essential for constraining
778 root water uptake dynamics but remain rare due to the labor-intensive and technically demanding nature of field
779 sampling and laboratory analysis (Landgraf et al., 2022; Sprenger et al., 2017). This scarcity hinders the spatial
780 and temporal resolution of observational data, limiting our ability to refine root water uptake processes in tracer-
781 aided models.

782 Upscaling from plot to landscape level remains complex due to spatial heterogeneity in vegetation, soils, and
783 topography. Addressing this requires spatially distributed modeling frameworks that can explicitly capture
784 heterogeneity in ecohydrological processes across different landscape units (van Huijgevoort et al., 2016; Kuppel
785 et al., 2018). Enhanced integration with remote sensing techniques can also help address these scaling limitations
786 by providing spatially continuous data on vegetation dynamics, soil moisture, and ET (Yang et al., 2023).
787 Incorporating ET observations, for instance, could strengthen model interpretation of flux dynamics. Currently,
788 key processes such as lateral subsurface flows and upward capillary fluxes are not explicitly represented in the
789 EcoPlot-iso model. Including these components, along with improved representation of groundwater-surface
790 water interactions, could improve simulations of hydrological connectivity and water storage dynamics.

791 It is important to note that the scenario framework presented here is intentionally exploratory and management-
792 oriented, rather than species-specific. While EcoPlot-iso captures key controls on water partitioning through
793 canopy structure, soil moisture dynamics, and tracer-based separation of fluxes, additional physiological traits—
794 such as stomatal regulation, vapor pressure deficit (VPD) sensitivity, and species-specific drought stress
795 strategies—are not explicitly represented. These processes are known to influence transpiration dynamics and
796 vegetation responses to drought, and their inclusion represents an important direction for future model
797 development. Accordingly, the results of this study are interpreted in a relative sense, emphasizing comparative
798 responses and management-relevant trade-offs rather than absolute or species-level predictions.

799 **6 Conclusion and Outlook**

800 The tracer-aided ecohydrological model EcoPlot-iso was applied to quantify how alternative forest management
801 scenarios influence long-term water partitioning and ecohydrological resilience in the drought-sensitive
802 Demnitzer Millcreek catchment (DMC), northeastern Germany. Baseline simulations for the period 2000–2024
803 were established at three forest sites (broadleaf forest, conifer forest, and agroforestry) and successfully
804 reproduced observed soil moisture and soil water isotope ($\delta^2\text{H}$) dynamics through a multi-criteria calibration
805 approach. A key development in this study was the integration of a depth-dependent root water uptake function,
806 which enable the representation of transpiration across soil layers associated with contrasting rooting distributions
807 and stand ages. Building on these baseline simulations, a generic scenario framework was applied to
808 systematically assess the effects of forest type, forest density, and rooting characteristics on evapotranspiration,
809 groundwater recharge, and soil moisture dynamics under contrasting dry and wet climatic conditions.

810 The results revealed clear trade-offs between evapotranspiration (ET) and groundwater recharge across different
811 forest management scenarios. On average, conifer forest exhibited higher ET, approximately 7–11% greater than
812 broadleaf forest and agroforestry, accompanied by reduced groundwater recharge, particularly during low-flow
813 periods. In contrast, agroforestry buffered drought stress, maintained lower soil moisture variability, and enhanced
814 groundwater recharge. Conifers showed the strongest soil moisture anomalies, indicating greater drought
815 sensitivity, while agroforests exhibited the most stable soil water storage. The middle soil layer (10–30 cm) was
816 identified as the most responsive zone, consistently exhibiting the largest anomalies due to its role as the dominant
817 root water uptake region supporting transpiration.

818 Beyond advancing process understanding, this study provided a practical and transferable framework for land
819 management. By incorporating key controls such as canopy properties and root distribution, EcoPlot-iso facilitates
820 an accessible means of assessing long-term land management impacts on landscape ecohydrology. The
821 visualization and decision-support framework developed here offers a transparent, scenario-based platform for
822 evaluating forest management strategies in climate-sensitive regions. These tools are well-suited for informing
823 resilient land use planning under increasing climate variability.

824 Looking ahead, future research could usefully aim to incorporate additional isotopic tracers—such as deeper soil
825 water (> 1 m), groundwater, and xylem water isotopes—to further constrain root water uptake functions and
826 capture their variability across species and hydroclimatic conditions. The integration of high-resolution remote
827 sensing data—particularly LiDAR for detailed characterization of forest structure—will enhance model

828 parameterization and improve the spatial representation of heterogeneity in canopy height, leaf area distribution,
829 and forest density. Advancing the EcoPlot-iso framework to incorporate lateral subsurface flows, groundwater
830 dynamics, and coupled land–atmosphere feedbacks will support broader applications, including the assessment of
831 large-scale land use change. Collectively, these developments will enhance model robustness and enable more
832 informed, resilient land and water management strategies under a warming climate.

833 **Code and data availability**

834 The data and code that support the findings of this study are available from the corresponding author upon
835 reasonable request.

836 **Author contribution**

837 CJ contributed to the methodology, software development, formal analysis, investigation, visualization, and
838 writing of the original draft. DT contributed to conceptualization, investigation, data curation, validation,
839 resources, project administration, and funding acquisition. SW contributed to methodology, investigation and data
840 curation. CB contributed to software, methodology, and resources. HL contributed to investigation, visualization
841 and validation. CS contributed to conceptualization, methodology, validation, investigation. All authors
842 contributed to writing – review and editing.

843 **Competing interests**

844 The authors declare that they have no conflict of interest.

845 **Acknowledgements**

846 Tetzlaff's contributions were partly funded through the WETSCAPES2.0 project (DFG TRR410/1 2025). Tetzlaff
847 also received funding from the "Wasserressourcenpreis 2024" awarded by the Rüdiger Kurt Bode-Foundation.
848 Contributions from Soulsby were supported by Leibnitz Association Germany in the project Wetland Restoration
849 in Peatlands. Laudon was funded by KAW 2018.0259 and 2023.0245, and Soulsby was also funded as an
850 International KSLA Guest Professor at SLU by the Wallenberg Foundation (WP2023-0001). Birkel would like to
851 thank the IGB for generously supporting him with a senior fellowship and the UCR for a sabbatical license. We
852 extend our appreciation to Benedikt Boesel and the team from the Finck Foundation (www.finck-stiftung.org) for
853 their collaborative support and for granting access to study sites. The authors are very grateful for the constructive
854 comments provided by the Editor, Prof. Dr. Anke Hildebrandt, and two anonymous reviewers.

855 **Reference**

- 856 Ault, T. R.: On the essentials of drought in a changing climate, *Science* (1979)., 368, 256–260,
857 <https://doi.org/10.1126/science.aaz5492>, 2020.
- 858 Birkel, C., Arciniega-Esparza, S., Maneta, M. P., Boll, J., Stevenson, J. L., Benegas-Negri, L., Tetzlaff, D., and
859 Soulsby, C.: Importance of measured transpiration fluxes for modelled ecohydrological partitioning in a

- 860 tropical agroforestry system, *Agric. For. Meteorol.*, 346, <https://doi.org/10.1016/j.agrformet.2023.109870>,
861 2024.
- 862 Birkel, C., Tetzlaff, D., Ring, A. M., and Soulsby, C.: Does high resolution in situ xylem and atmospheric vapor
863 isotope data help improve modeled estimates of ecohydrological partitioning?, *Agric. For. Meteorol.*, 365,
864 <https://doi.org/10.1016/j.agrformet.2025.110467>, 2025.
- 865 Bonan, G. B.: Forests and climate change: Forcings, feedbacks, and the climate benefits of forests, *Science* (1979).,
866 320, 1444–1449, <https://doi.org/10.1126/science.1155121>, 2008.
- 867 Bosch, J. M. and Hewlett, J. D.: A review of catchment experiments to determine the effect of vegetation changes
868 on water yield and evapotranspiration, *J. Hydrol. (Amst.)*, 55, 3–23, [https://doi.org/10.1016/0022-1694\(82\)90117-2](https://doi.org/10.1016/0022-1694(82)90117-2), 1982.
- 870 Brauman, K. A., Freyberg, D. L., and Daily, G. C.: Forest structure influences on rainfall partitioning and cloud
871 interception: A comparison of native forest sites in Kona, Hawai'i, *Agric. For. Meteorol.*, 150,
872 <https://doi.org/10.1016/j.agrformet.2009.11.011>, 2010.
- 873 Brown, A. E., Zhang, L., McMahon, T. A., Western, A. W., and Vertessy, R. A.: A review of paired catchment
874 studies for determining changes in water yield resulting from alterations in vegetation, *J. Hydrol. (Amst.)*, 310,
875 28–61, <https://doi.org/10.1016/j.jhydrol.2004.12.010>, 2005.
- 876 Brown, A. E., Western, A. W., McMahon, T. A., and Zhang, L.: Impact of forest cover changes on annual
877 streamflow and flow duration curves, *J. Hydrol. (Amst.)*, 483, <https://doi.org/10.1016/j.jhydrol.2012.12.031>,
878 2013.
- 879 Calder, I. R.: Water use by forests, limits and controls, in: *Tree Physiology*, <https://doi.org/10.1093/treephys/18.8-9.625>, 1998.
- 881 Demir, G., Guswa, A. J., Filipzik, J., Metzger, J. C., Römermann, C., and Hildebrandt, A.: Root water uptake
882 patterns are controlled by tree species interactions and soil water variability, *Hydrol. Earth Syst. Sci.*, 28, 1441–
883 1461, <https://doi.org/10.5194/hess-28-1441-2024>, 2024.
- 884 Ellison, D., Fitter, M. N., and Bishop, K.: On the forest cover-water yield debate: From demand- to supply-side
885 thinking, *Glob. Chang. Biol.*, 18, <https://doi.org/10.1111/j.1365-2486.2011.02589.x>, 2012.
- 886 Emerman, S. H. and Dawson, T. E.: Hydraulic lift and its influence on the water content of the rhizosphere: An
887 example from sugar maple, *Acer saccharum*, *Oecologia*, 108, <https://doi.org/10.1007/BF00334651>, 1996.
- 888 Estrela, T. and Vargas, E.: Drought Management Plans in the European Union. The Case of Spain, *Water
889 Resources Management*, 26, 1537–1553, <https://doi.org/10.1007/s11269-011-9971-2>, 2012.
- 890 Evaristo, J. and McDonnell, J. J.: Prevalence and magnitude of groundwater use by vegetation: A global stable
891 isotope meta-analysis, *Sci. Rep.*, 7, <https://doi.org/10.1038/srep44110>, 2017.
- 892 Falkenmark, M. and Rockström, J.: The New Blue and Green Water Paradigm: Breaking New Ground for Water
893 Resources Planning and Management, *J. Water Resour. Plan. Manag.*, 132, [https://doi.org/10.1061/\(asce\)0733-9496\(2006\)132:3\(129\)](https://doi.org/10.1061/(asce)0733-9496(2006)132:3(129)), 2006.
- 895 Fatichi, S., Ivanov, V. Y., and Caporali, E.: A mechanistic ecohydrological model to investigate complex
896 interactions in cold and warm water-controlled environments: 1. Theoretical framework and plot-scale analysis,
897 *J. Adv. Model. Earth Syst.*, 4, <https://doi.org/10.1029/2011MS000086>, 2012.
- 898 Filoso, S., Bezerra, M. O., Weiss, K. C. B., and Palmer, M. A.: Impacts of forest restoration on water yield: A
899 systematic review, *PLoS One*, 12, <https://doi.org/10.1371/journal.pone.0183210>, 2017.
- 900 Gelbrecht, J., Driescher, E., Lademann, H., Schönfelder, J., and Exner, H.-J.: Diffuse nutrient impact on surface
901 water bodies and its abatement by restoration measures in a small catchment area in North-East Germany,
902 *Water Science and Technology*, 33, <https://doi.org/10.2166/wst.1996.0501>, 1996.

- 903 Gelbrecht, J., Lengsfeld, H., Pöthig, R., and Opitz, D.: Temporal and spatial variation of phosphorus input,
 904 retention and loss in a small catchment of NE Germany, *J. Hydrol. (Amst.)*, 304, 151–165,
 905 <https://doi.org/10.1016/j.jhydrol.2004.07.028>, 2005.
- 906 Geris, J., Tetzlaff, D., McDonnell, J., and Soulsby, C.: The relative role of soil type and tree cover on water storage
 907 and transmission in northern headwater catchments, *Hydrol. Process.*, 29, <https://doi.org/10.1002/hyp.10289>,
 908 2015.
- 909 Guswa, A. J., Tetzlaff, D., Selker, J. S., Carlyle-Moses, D. E., Boyer, E. W., Bruen, M., Cayuela, C., Creed, I. F.,
 910 van de Giesen, N., Grasso, D., Hannah, D. M., Hudson, J. E., Hudson, S. A., Iida, S., Jackson, R. B., Katul, G.
 911 G., Kumagai, T., Llorens, P., Lopes Ribeiro, F., Michalzik, B., Nanko, K., Oster, C., Pataki, D. E., Peters, C.
 912 A., Rinaldo, A., Sanchez Carretero, D., Trifunovic, B., Zalewski, M., Haagsma, M., and Levia, D. F.:
 913 Advancing ecohydrology in the 21st century: A convergence of opportunities, <https://doi.org/10.1002/eco.2208>,
 914 1 June 2020.
- 915 Hersbach, H., Bell, B., Berrisford, P., Hirahara, S., Horányi, A., Muñoz-Sabater, J., Nicolas, J., Peubey, C., Radu,
 916 R., Schepers, D., Simmons, A., Soci, C., Abdalla, S., Abellan, X., Balsamo, G., Bechtold, P., Biavati, G., Bidlot,
 917 J., Bonavita, M., De Chiara, G., Dahlgren, P., Dee, D., Diamantakis, M., Dragani, R., Flemming, J., Forbes, R.,
 918 Fuentes, M., Geer, A., Haimberger, L., Healy, S., Hogan, R. J., Hólm, E., Janisková, M., Keeley, S., Laloyaux,
 919 P., Lopez, P., Lupu, C., Radnoti, G., de Rosnay, P., Rozum, I., Vamborg, F., Villaume, S., and Thépaut, J.-N.:
 920 The ERA5 global reanalysis, *Quarterly Journal of the Royal Meteorological Society*, 146, 1999–2049,
 921 <https://doi.org/https://doi.org/10.1002/qj.3803>, 2020.
- 922 Hibbert, A. R.: Forest Treatment Effects on Water Yield, in: *International Symposium For Hydrology*, 527–543,
 923 1967.
- 924 van Huijgevoort, M. H. J., Tetzlaff, D., Sutanudjaja, E. H., and Soulsby, C.: Using high resolution tracer data to
 925 constrain water storage, flux and age estimates in a spatially distributed rainfall-runoff model, *Hydrol. Process.*,
 926 30, 4761–4778, <https://doi.org/10.1002/hyp.10902>, 2016.
- 927 Huntington, T. G.: Evidence for intensification of the global water cycle: Review and synthesis, *J. Hydrol. (Amst.)*,
 928 319, 83–95, <https://doi.org/10.1016/j.jhydrol.2005.07.003>, 2006.
- 929 Kleine, L., Tetzlaff, D., Smith, A., Dubbert, M., and Soulsby, C.: Modelling ecohydrological feedbacks in forest
 930 and grassland plots under a prolonged drought anomaly in Central Europe 2018–2020, *Hydrol. Process.*, 35,
 931 <https://doi.org/10.1002/hyp.14325>, 2021.
- 932 Kling, H., Fuchs, M., and Paulin, M.: Runoff conditions in the upper Danube basin under an ensemble of climate
 933 change scenarios, *J. Hydrol. (Amst.)*, 424–425, <https://doi.org/10.1016/j.jhydrol.2012.01.011>, 2012.
- 934 Kool, D., Agam, N., Lazarovitch, N., Heitman, J. L., Sauer, T. J., and Ben-Gal, A.: A review of approaches for
 935 evapotranspiration partitioning, *Agric. For. Meteorol.*, 184, 56–70,
 936 <https://doi.org/10.1016/j.agrformet.2013.09.003>, 2014.
- 937 Kuppel, S., Tetzlaff, D., Maneta, M. P., and Soulsby, C.: EcH2O-iso 1.0: Water isotopes and age tracking in a
 938 process-based, distributed ecohydrological model, *Geosci. Model Dev.*, 11, 3045–3069,
 939 <https://doi.org/10.5194/gmd-11-3045-2018>, 2018.
- 940 Landgraf, J., Tetzlaff, D., Wu, S., Freymüller, J., and Soulsby, C.: Using stable water isotopes to understand
 941 ecohydrological partitioning under contrasting land uses in a drought-sensitive rural, lowland catchment, in:
 942 *Hydrological Processes*, <https://doi.org/10.1002/hyp.14779>, 2022.
- 943 Landgraf, J., Tetzlaff, D., Birkel, C., Stevenson, J. L., and Soulsby, C.: Assessing land use effects on
 944 ecohydrological partitioning in the critical zone through isotope-aided modelling, *Earth Surf. Process. Landf.*,
 945 48, 3199–3219, <https://doi.org/10.1002/esp.5691>, 2023.
- 946 Luo, S., Tetzlaff, D., Smith, A., and Soulsby, C.: Assessing impacts of alternative land use strategies on water
 947 partitioning, storage and ages in drought-sensitive lowland catchments using tracer-aided ecohydrological
 948 modelling, *Hydrol. Process.*, 38, <https://doi.org/10.1002/hyp.15126>, 2024.

- 949 Mahmood, R., Pielke, R. A., Hubbard, K. G., Niyogi, D., Dirmeyer, P. A., McAlpine, C., Carleton, A. M., Hale,
950 R., Gameda, S., Beltrán-Przekurat, A., Baker, B., Mcnider, R., Legates, D. R., Shepherd, M., Du, J., Blanken,
951 P. D., Frauenfeld, O. W., Nair, U. S., and Fall, S.: Land cover changes and their biogeophysical effects on
952 climate, *International Journal of Climatology*, 34, <https://doi.org/10.1002/joc.3736>, 2014.
- 953 McKay, M. D., Beckman, R. J., and Conover, W. J.: Comparison of three methods for selecting values of input
954 variables in the analysis of output from a computer code, *Technometrics*, 21,
955 <https://doi.org/10.1080/00401706.1979.10489755>, 1979.
- 956 Neill, A. J., Birkel, C., Maneta, M. P., Tetzlaff, D., and Soulsby, C.: Structural changes to forests during
957 regeneration affect water flux partitioning, water ages and hydrological connectivity: Insights from tracer-aided
958 ecohydrological modelling, *Hydrol. Earth Syst. Sci.*, 25, 4861–4886, [https://doi.org/10.5194/hess-25-4861-](https://doi.org/10.5194/hess-25-4861-2021)
959 2021, 2021.
- 960 Orth, R. and Destouni, G.: Drought reduces blue-water fluxes more strongly than green-water fluxes in Europe,
961 *Nat. Commun.*, 9, <https://doi.org/10.1038/s41467-018-06013-7>, 2018.
- 962 Penna, D., Hopp, L., Scandellari, F., Allen, S. T., Benetton, P., Beyer, M., Geris, J., Klaus, J., Marshall, J. D.,
963 Schwendenmann, L., Volkmann, T. H. M., Von Freyberg, J., Amin, A., Ceperley, N., Engel, M., Frentress, J.,
964 Giambastiani, Y., McDonnell, J. J., Zuecco, G., Llorens, P., Siegwolf, R. T. W., Dawson, T. E., and Kirchner,
965 J. W.: Ideas and perspectives: Tracing terrestrial ecosystem water fluxes using hydrogen and oxygen stable
966 isotopes - Challenges and opportunities from an interdisciplinary perspective, *Biogeosciences*, 15,
967 <https://doi.org/10.5194/bg-15-6399-2018>, 2018.
- 968 Pielke, R. A., Pitman, A., Niyogi, D., Mahmood, R., McAlpine, C., Hossain, F., Goldewijk, K. K., Nair, U., Betts,
969 R., Fall, S., Reichstein, M., Kabat, P., and de Noblet, N.: Land use/land cover changes and climate: Modeling
970 analysis and observational evidence, <https://doi.org/10.1002/wcc.144>, 2011.
- 971 Quandt, A., Neufeldt, H., and Gorman, K.: Climate change adaptation through agroforestry: opportunities and
972 gaps, <https://doi.org/10.1016/j.cosust.2022.101244>, 2023.
- 973 Ricci, G. F., De Girolamo, A. M., and Gentile, F.: Modeling the Effect of Different Management Practices for
974 Soil Erosion Control in a Mediterranean Watershed, *Lecture Notes in Civil Engineering*, 67, 125–132,
975 https://doi.org/10.1007/978-3-030-39299-4_14, 2020.
- 976 Rothfuss, Y. and Javaux, M.: Reviews and syntheses: Isotopic approaches to quantify root water uptake: A review
977 and comparison of methods, *Biogeosciences*, 14, <https://doi.org/10.5194/bg-14-2199-2017>, 2017.
- 978 Shen, H., Tolson, B. A., and Mai, J.: Time to Update the Split-Sample Approach in Hydrological Model
979 Calibration, *Water Resour. Res.*, 58, <https://doi.org/10.1029/2021WR031523>, 2022.
- 980 Smith, A., Tetzlaff, D., Gelbrecht, J., Kleine, L., and Soulsby, C.: Riparian wetland rehabilitation and beaver re-
981 colonization impacts on hydrological processes and water quality in a lowland agricultural catchment, *Science*
982 *of the Total Environment*, 699, <https://doi.org/10.1016/j.scitotenv.2019.134302>, 2020.
- 983 Smith, A., Tetzlaff, D., Kleine, L., Maneta, M., and Soulsby, C.: Quantifying the effects of land use and model
984 scale on water partitioning and water ages using tracer-aided ecohydrological models, *Hydrol. Earth Syst. Sci.*,
985 25, 2239–2259, <https://doi.org/10.5194/hess-25-2239-2021>, 2021.
- 986 Soulsby, C., Birkel, C., Geris, J., Dick, J., Tunaley, C., and Tetzlaff, D.: Stream water age distributions controlled
987 by storage dynamics and nonlinear hydrologic connectivity: Modeling with high-resolution isotope data, *Water*
988 *Resour. Res.*, 51, <https://doi.org/10.1002/2015WR017888>, 2015.
- 989 Sprenger, M., Tetzlaff, D., and Soulsby, C.: Soil water stable isotopes reveal evaporation dynamics at the soil-
990 plant-atmosphere interface of the critical zone, *Hydrol. Earth Syst. Sci.*, 21, [https://doi.org/10.5194/hess-21-](https://doi.org/10.5194/hess-21-3839-2017)
991 3839-2017, 2017.
- 992 Sterling, S. M., Ducharne, A., and Polcher, J.: The impact of global land-cover change on the terrestrial water
993 cycle, *Nat. Clim. Chang.*, 3, <https://doi.org/10.1038/nclimate1690>, 2013.

- 994 Stevenson, J. L., Birkel, C., Comte, J. C., Tetzlaff, D., Marx, C., Neill, A., Maneta, M., Boll, J., and Soulsby, C.:
 995 Quantifying heterogeneity in ecohydrological partitioning in urban green spaces through the integration of
 996 empirical and modelling approaches, *Environ. Monit. Assess.*, 195, [https://doi.org/10.1007/s10661-023-11055-](https://doi.org/10.1007/s10661-023-11055-6)
 997 6, 2023.
- 998 Tague, C. L. and Band, L. E.: RHESSys: Regional Hydro-Ecologic Simulation System—An Object-Oriented
 999 Approach to Spatially Distributed Modeling of Carbon, Water, and Nutrient Cycling, *Earth Interact.*, 8,
 1000 [https://doi.org/10.1175/1087-3562\(2004\)8<1:rrhss0>2.0.co;2](https://doi.org/10.1175/1087-3562(2004)8<1:rrhss0>2.0.co;2), 2004.
- 1001 Tetzlaff, D., Carey, S. K., McNamara, J. P., Laudon, H., and Soulsby, C.: The essential value of long-term
 1002 experimental data for hydrology and water management, <https://doi.org/10.1002/2017WR020838>, 1 April 2017.
- 1003 Tetzlaff, D., Laudon, H., Luo, S., and Soulsby, C.: Ecohydrological resilience and the landscape water storage
 1004 continuum in droughts, *Nature Water*, 2, 915–918, <https://doi.org/10.1038/s44221-024-00300-y>, 2024.
- 1005 Trenberth, K. E.: Changes in precipitation with climate change, *Clim. Res.*, 47, 123–138,
 1006 <https://doi.org/10.3354/cr00953>, 2011.
- 1007 Wang-Erlandsson, L., Van Der Ent, R. J., Gordon, L. J., and Savenije, H. H. G.: Contrasting roles of interception
 1008 and transpiration in the hydrological cycle - Part 1: Temporal characteristics over land, *Earth System Dynamics*,
 1009 5, <https://doi.org/10.5194/esd-5-441-2014>, 2014.
- 1010 te Wierik, S. A., Cammeraat, E. L. H., Gupta, J., and Artzy-Randrup, Y. A.: Reviewing the Impact of Land Use
 1011 and Land-Use Change on Moisture Recycling and Precipitation Patterns, *Water Resour. Res.*, 57,
 1012 <https://doi.org/10.1029/2020WR029234>, 2021.
- 1013 Wu, S., Tetzlaff, D., Goldhammer, T., and Soulsby, C.: Hydroclimatic variability and riparian wetland restoration
 1014 control the hydrology and nutrient fluxes in a lowland agricultural catchment, *J. Hydrol. (Amst.)*, 603,
 1015 <https://doi.org/10.1016/j.jhydrol.2021.126904>, 2021.
- 1016 Wu, S., Tetzlaff, D., Yang, X., Smith, A., and Soulsby, C.: Integrating Tracers and Soft Data Into Multi-Criteria
 1017 Calibration: Implications From Distributed Modeling in a Riparian Wetland, *Water Resour. Res.*, 59,
 1018 <https://doi.org/10.1029/2023WR035509>, 2023.
- 1019 Wu, S., Tetzlaff, D., Beven, K., and Soulsby, C.: DREAM(LoAX): Simultaneous Calibration and Diagnosis for
 1020 Tracer-Aided Ecohydrological Models Under the Equifinality Thesis, *Water Resour. Res.*, 61,
 1021 e2024WR038779, <https://doi.org/https://doi.org/10.1029/2024WR038779>, 2025.
- 1022 Yang, X., Tetzlaff, D., Müller, C., Knöller, K., Borchardt, D., and Soulsby, C.: Upscaling Tracer-Aided
 1023 Ecohydrological Modeling to Larger Catchments: Implications for Process Representation and Heterogeneity
 1024 in Landscape Organization, *Water Resour. Res.*, 59, <https://doi.org/10.1029/2022WR033033>, 2023.
- 1025 Ying, Z., Tetzlaff, D., Comte, J.-C., Wu, S., and Soulsby, C.: Storage Dynamics and Groundwater–Surface Water
 1026 Interactions in a Drought Sensitive Lowland Catchment: Process-Based Modelling as a Learning Tool, *Hydrol.*
 1027 *Process.*, 39, e70141, <https://doi.org/https://doi.org/10.1002/hyp.70141>, 2025.
- 1028 Yuan, X., Wang, Y., Ji, P., Wu, P., Sheffield, J., and Otkin, J. A.: A global transition to flash droughts under
 1029 climate change, *Science (1979)*, 380, <https://doi.org/10.1126/science.abn6301>, 2023.
- 1030 Zhang, L., Dawes, W. R., and Walker, G. R.: Response of mean annual evapotranspiration to vegetation changes
 1031 at catchment scale, *Water Resour. Res.*, 37, <https://doi.org/10.1029/2000WR900325>, 2001.
- 1032